AL/CF-TR-1994-0115

ARMSTRONG LABORATORY

IMAGE QUALITY METRICS FOR COLOR CRT DISPLAYS (U)

Robert J. Beaton
Willard W. Farley

KEYSTONE ENGINEERING LIMITED
BLACKSBURG, VIRGINIA

AUGUST 1994

INTERIM REPORT FOR THE PERIOD JANUARY 1993 TO JULY 1993

Approved for public release; distribution is unlimited

AIR FORCE MATERIEL COMMAND
WRIGHT-PATTERSON AIR FORCE BASE, OHIO 45433-7022

NOTICES

When US Government drawings, specifications, or other data are used for any purpose other than a definitely related Government procurement operation, the Government thereby incurs no responsibility nor any obligation whatsoever, and the fact that the Government may have formulated, furnished, or in any way supplied the said drawings, specifications, or other data, is not to be regarded by implication or otherwise, as in any manner licensing the holder or any other person or corporation, or conveying any rights or permission to manufacture, use, or sell any patented invention that may in any way be related thereto.

Please do not request copies of this report from the Armstrong Laboratory. Additional copies may be purchased from:

National Technical Information Service
5285 Port Royal Road
Springfield, Virginia 22161

Federal Government agencies and their contractors registered with the Defense Technical Information Center should direct requests for copies of this report to:

Defense Technical Information Center
Cameron Station
Alexandria, Virginia 22314

DISCLAIMER

This Technical Report is published as received and has not been edited by the Technical Editing Staff of the Armstrong Laboratory.

TECHNICAL REVIEW AND APPROVAL

AL/CF-TR-1994-0115

This report has been reviewed by the Office of Public Affairs (PA) and is releasable to the National Technical Information Service (NTIS). At NTIS, it will be available to the general public, including foreign nations.

This technical report has been reviewed and is approved for publication.

FOR THE COMMANDER

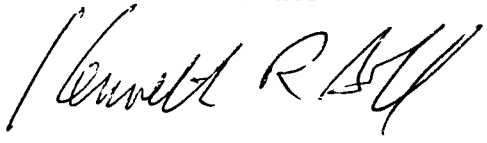

KENNETH R. BOFF, Chief
Human Engineering Division
Armstrong Laboratory

REPORT DOCUMENTATION PAGE

Form Approved
OMB No. 0704-0188

1. AGENCY USE ONLY (Leave blank)	2. REPORT DATE	3. REPORT TYPE AND DATES COVERED
	August 1994	Interim Report Jan 93 - Jul 93

4. TITLE AND SUBTITLE

Image Quality Metrics for Color CRT Displays

5. FUNDING NUMBERS

C: F33615-89-C-0532
PE - 62202F
PR - 7184
TA - 10
WU - 44

6. AUTHOR(S)

Robert J. Beaton, PhD
Willard W. Farley

7. PERFORMING ORGANIZATION NAME(S) AND ADDRESS(ES)

Keystone Engineering Limited
P. O. Box 11046
Blacksburg VA 24062-1046

8. PERFORMING ORGANIZATION REPORT NUMBER

9. SPONSORING/MONITORING AGENCY NAME(S) AND ADDRESS(ES)

Armstrong Laboratory, Crew Systems Directorate
Human Engineering Division
Human Systems Center
Air Force Materiel Command
Wright-Patterson AFB OH 45433-7022

10. SPONSORING/MONITORING AGENCY REPORT NUMBER

AL/CF-TR-1994-0115

11. SUPPLEMENTARY NOTES

12a. DISTRIBUTION/AVAILABILITY STATEMENT

Approved for public release; distribution is unlimited.

12b. DISTRIBUTION CODE

13. ABSTRACT *(Maximum 200 words)*

This study explores several different image quality metrics currently employed by the visual display community in the context of color CRT display technology. The specific techniques included in the study are the Modulation Transfer Function, the Contrast Threshold/Sensitivity Function, the Modulation Transfer Function Area, the Integrated Contrast Sensitivity metric, and the Square-Root Integral metric. These metrics include and are based on visual psychometric data and suggest that operator performance may be predicted from the objective, image quality data.

14. SUBJECT TERMS

Displays, image quality metrics, visual thresholds, visual psychometrics, color, cathode ray tubes

15. NUMBER OF PAGES
89

16. PRICE CODE

17. SECURITY CLASSIFICATION OF REPORT	18. SECURITY CLASSIFICATION OF THIS PAGE	19. SECURITY CLASSIFICATION OF ABSTRACT	20. LIMITATION OF ABSTRACT
UNCLASSIFIED	UNCLASSIFIED	UNCLASSIFED	UNLIMITED

THIS PAGE INTENTIONALLY LEFT BLANK

Preface

This report was prepared by Keystone Engineering Limited, Blacksburg, Virginia for the Armstrong Laboratory, Human Systems Division, United States Air Force, Wright-Patterson AFB, Ohio 45433-6573 under Contract No. F33615-89-C-0532 (Subcontract No. 07-014-43S). Mr. Robert Linhart was the U.S. Air Force Contract Monitor and Mr. Gilbert G. Kuperman was the Work Unit Manager. This report documents the project activities for the contract period January 1993 to July 1993. Robert J Beaton was the Principal Investigator.

Table of Contents

List of Tables

List of Figures

List of Symbols

$d(x,y)$	Two Dimensional Delta or Sampling Function
Y	Line-to-Dot Phase or Line-to-Stripe Phase
f_b	Blue Misconvergence
f_r	Red Misconvergence
$A(x,y)$	Two Dimensional Aperture Function
a_h	Measurement System Aperture Height
a_w	Measurement System Aperture Width
$AL(w)$	Modulation of Alias Frequency (w)
$D_b(x,y)$	Two Dimensional Blue Dot Function
$D_g(x,y)$	Two Dimensional Green Dot Function
$D_r(x,y)$	Two Dimensional Red Dot Function
$D(x,y)$	Two Dimensional General Dot Function
I_b	Blue Phosphor Intensity
I_g	Green Phosphor Intensity
I_r	Red Phosphor Intensity
$L_b(x)$	One Dimensional Blue Location Equation
$L_g(x)$	One Dimensional Green Location Equation
$L_r(x)$	One Dimensional Red Location Equation
$L_b(x,y)$	Two Dimensional Blue Location Equation
$L_g(x,y)$	Two Dimensional Green Location Equation
$L_r(x,y)$	Two Dimensional Red Location Equation
$Line_b(x,y)$	Two Dimensional Blue Line Function for a Single Line
$Line_g(x,y)$	Two Dimensional Green Line Function for a Single Line
$Line_r(x,y)$	Two Dimensional Red Line Function for a Single Line
$LP_b(x,y)$	Two Dimensional Blue Line Pattern Function for On-Off Line Pattern
$LP_g(x,y)$	Two Dimensional Green Line Pattern Function for On-Off Line Pattern
$LP_r(x,y)$	Two Dimensional Red Line Pattern Function for On-Off Line Pattern
$LP_b(x)$	Blue Line Pattern Function for On-Off Line Pattern
$LP_g(x)$	Green Line Pattern Function for On-Off Line Pattern
$LP_r(x)$	Red Line Pattern Function for On-Off Line Pattern
LSF	Line Spread Function
LSF_b	Blue Line Spread Function
LSF_g	Green Line Spread Function
LSF_r	Red Line Spread Function

mod2()	Modulo Function (Returns 0 for Even Argument and 1 for Odd Argument)
P	Shadow Mask Pitch
P_h	Horizontal Pitch of adjacent phosphor dots of the same color
$PMLP_b$	Pre-Mask Line Pattern for Blue Lines
$PMLP_g$	Pre-Mask Line Pattern for Green Lines
$PMLP_r$	Pre-Mask Line Pattern for Red Lines
PMLSF	Pre-Mask Line Spread Function
$PMLSF_r$	Red Pre-Mask Line Spread Function
$PMLSF_g$	Green Pre-Mask Line Spread Function
$PMLSF_b$	Blue Pre-Mask Line Spread Function
P_v	Vertical Pitch of adjacent rows of phosphor dots
r_b	Blue Phosphor Dot Radius
r_g	Green Phosphor Dot Radius
r_r	Red Phosphor Dot Radius
s_b	Blue Phosphor Stripe Width
s_g	Green Phosphor Stripe Width
s_r	Red Phosphor Stripe Width
$S_b(x)$	Blue Phosphor Stripe Function
$S_g(x)$	Green Phosphor Stripe Function
$S_r(x)$	Red Phosphor Stripe Function
S(x)	General Phosphor Stripe Function
$SS_b(x)$	Blue Stripe Screen Sampling Function
$SS_g(x)$	Green Stripe Screen Sampling Function
$SS_r(x)$	Red Stripe Screen Sampling Function
$SS_b(x,y)$	Blue Dot Screen Sampling Function
$SS_g(x,y)$	Green Dot Screen Sampling Function
$SS_r(x,y)$	Red Dot Screen Sampling Function
STAV	Super-Threshold Alias Value
w_b	Blue Line Width at Half Maximum
w_g	Green Line Width at Half Maximum
w_r	Red Line Width at Half Maximum

Section I. Introduction

The Modulation Transfer Function (MTF) is a fundamental representation of the imaging capacity of a visual display device (Beaton, 1984). It quantifies the amount of luminance energy that a visual display can transmit for each spatial frequency component in an input signal (image). The MTF has been used to characterize the image transmission properties of optical lens systems, photographic films, continuous tone hard-copy printers, and a wide variety of electro-optical displays.

Across the applications of the MTF, it is assumed that the image-forming surface of the device is spatially continuous and homogeneous. This assumption is valid for most optical lens systems, and it is considered as valid for most photographic media since the image-forming surface consists of very small light reflecting particles. However, other types of display devices have discretely sampled image-forming surfaces. For example, Cathode Ray Tube (CRT) and Flat Panel (FP) devices use a matrix of discrete picture elements (i.e., phosphors dots, sub-pixel elements) to produce a viewable image. This work develops and tests a method to extend the MTF concept to these types of spatially sampled display devices.

Previous work in this area has attempted to describe the imaging capacity of spatially sampled displays by evaluating the amount of usable luminance modulation produced by a one-pixel on/one-pixel off (On-Off) line pattern transmitted through the display system (O'Callaghan and Veron, 1987; Veron and O'Callaghan, 1987; O'Callaghan and Veron, 1989). Specifically, the amount of usable luminance modulation is computed from a measured On-Off pattern after filtering it by the spatial frequency transfer function of an ideal observer. Unfortunately, this approach is susceptible to errors stemming from the sampling artifacts in the measured luminance pattern.

An alternative approach to representing the imaging capacity of spatially sampled displays is presented here. The approach is based on the notion of a sampling criteria, which sets an upper bound on the useful range of spatial frequencies used in the MTF calculations. The applications of this approach to image quality metric calculations and photometric measurement systems are discussed.

Section II. Background

This section reviews the major types of CRT technologies and some of the traditional MTF-based image quality metrics used in the visual display engineering community.

II.1 Color CRT Technologies

There are several types of CRT displays (see Figure 1). In general, CRT displays are categorized as monochrome or color devices. Monochrome CRTs employ a single electron gun and a continuous deposition of phosphor to produce a viewable image. The image is formed by electrons exciting the phosphor in a regular scan pattern, often called a raster structure. Monochrome CRTs can render images at various luminance intensity levels (i.e., shades of gray); but, the color of the image is determined by the type of phosphor used.

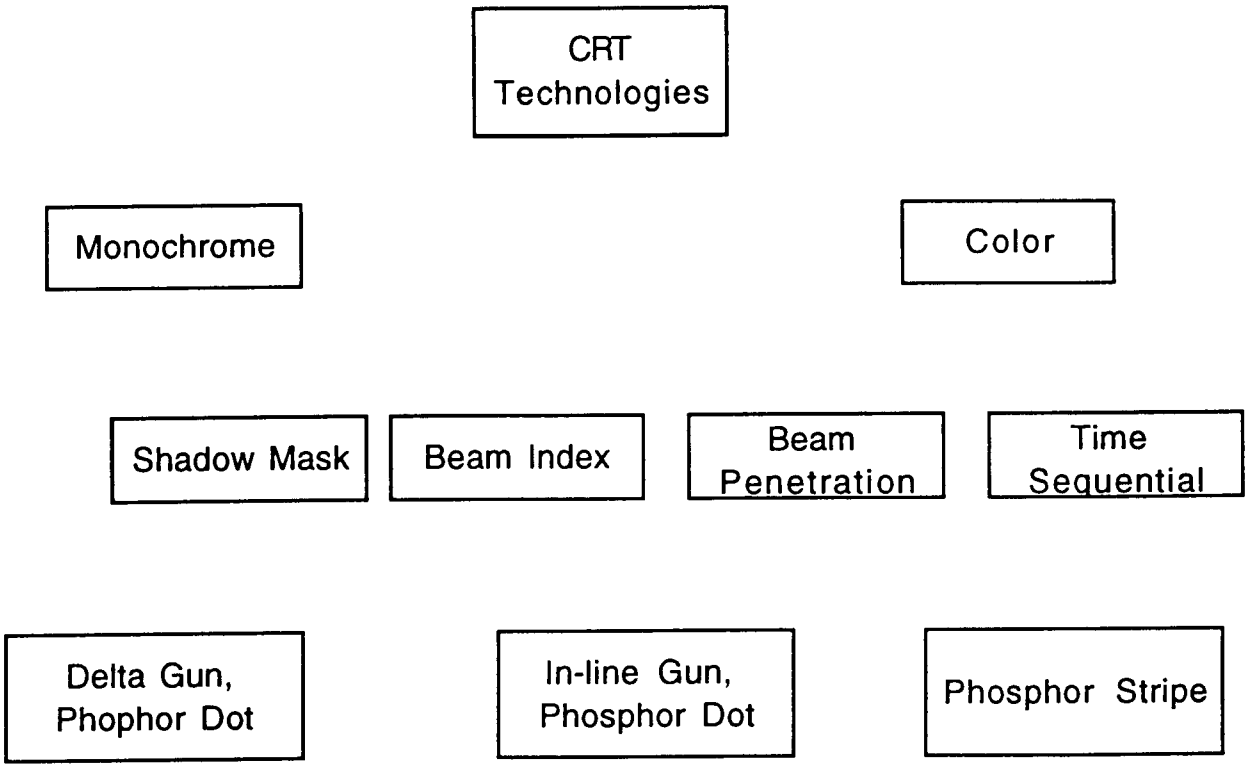

Figure 1. Types of CRT display technologies.

Color CRTs use multiple electron guns to excite different types (colors) of phosphor on the image-forming surface. There are several types of color CRT displays: shadow mask, beam penetration, beam index, and time sequential. The shadow mask CRTs

are most common in commercial markets, whereas the remaining types of color CRTs are used in special-purpose applications. Two types of shadow mask CRTs are described below.

II.1.a Phosphor Dot CRTs. Most color CRTs use a phosphor dot shadow mask technology. Figure 2 illustrates the major components in a delta gun version of this type of color CRT. As shown in Figure 2, three electron guns are positioned at the vertices of an equilateral triangle; hence the term delta gun configuration. The shadow mask is located between the electron guns and the image-forming phosphor surface, and it consists of uniformly spaced holes (apertures). The image-forming surface consists of uniformly placed dots of red-, green-, and blue-colored phosphor. Electrons from each gun pass through the mask holes to excite the phosphor dots; one gun excites the red phosphor dots, another one excites the green phosphor dots, and the third gun excites the blue phosphor dots. The electron beams emerging a single illuminate several shadow mask holes and groupings or triads of the colored phosphor dots.

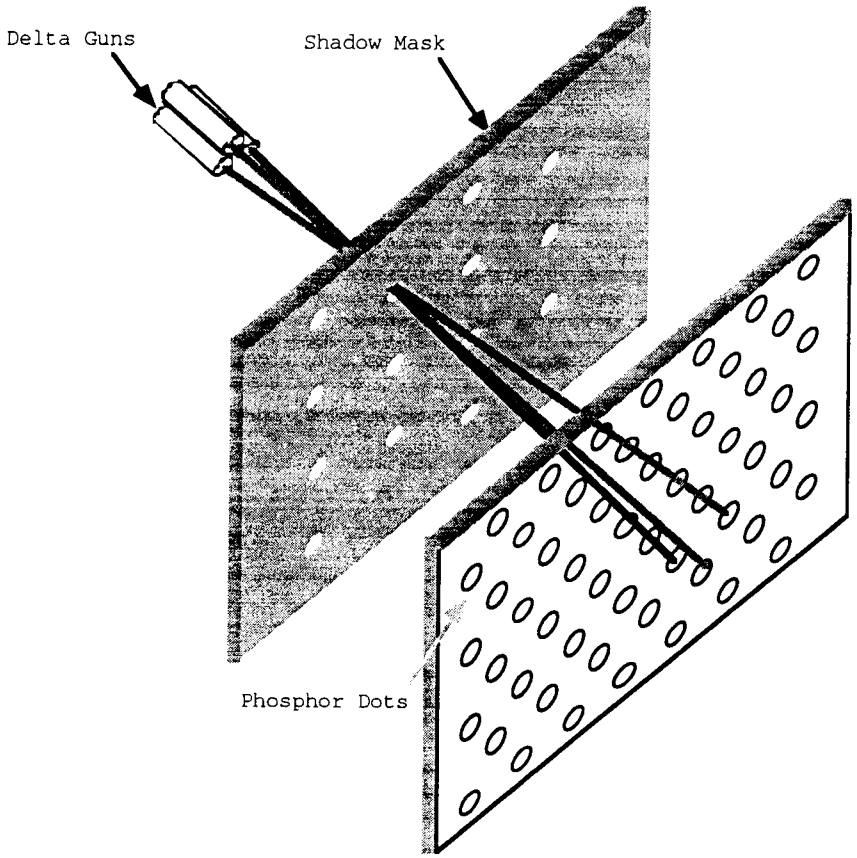

Figure 2. Illustration of delta-gun phosphor dot CRT.

Figure 3 shows the geometric arrangement of phosphor dots and shadow mask holes in a delta gun CRT. The Pitch (P) of the shadow mask is defined as the vertical distance between horizontally aligned mask holes.

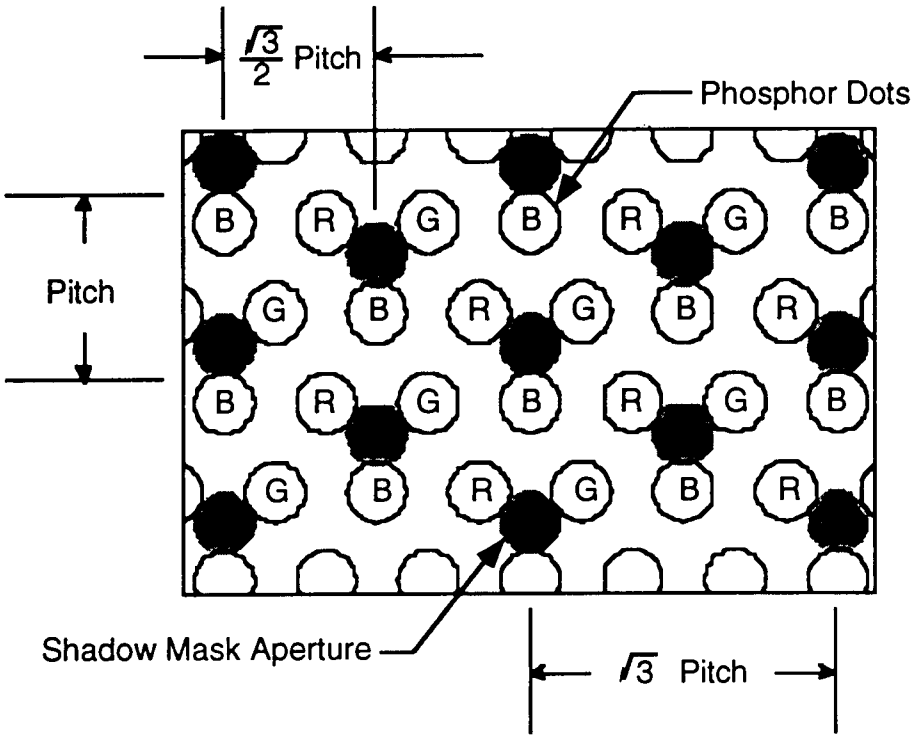

Figure 3. Geometry of delta-gun phosphor dot CRT.

The vertical distance between rows of phosphor dots is given as:

$$P_v = \frac{1}{2} P \qquad \text{(Eq. 1)}$$

in which
P_d is the vertical pitch of the phosphor dots.

Similarly, the horizontal distance between same-colored phosphor dots is given as:

$$P_h = \sqrt{3}\, P \qquad \text{(Eq. 2)}$$

in which
P_h is the horizontal pitch of phosphor dots of the same color.

Figure 4 illustrates another configuration of phosphor dot CRTs called the in-line gun design. The electron beams emitted by the in-line guns pass through the shadow mask holes to illuminate the red-, green-, and blue-colored phosphor dots. However, the in-line CRT electron guns are arranged in a horizontal line, rather than in a delta configuration.

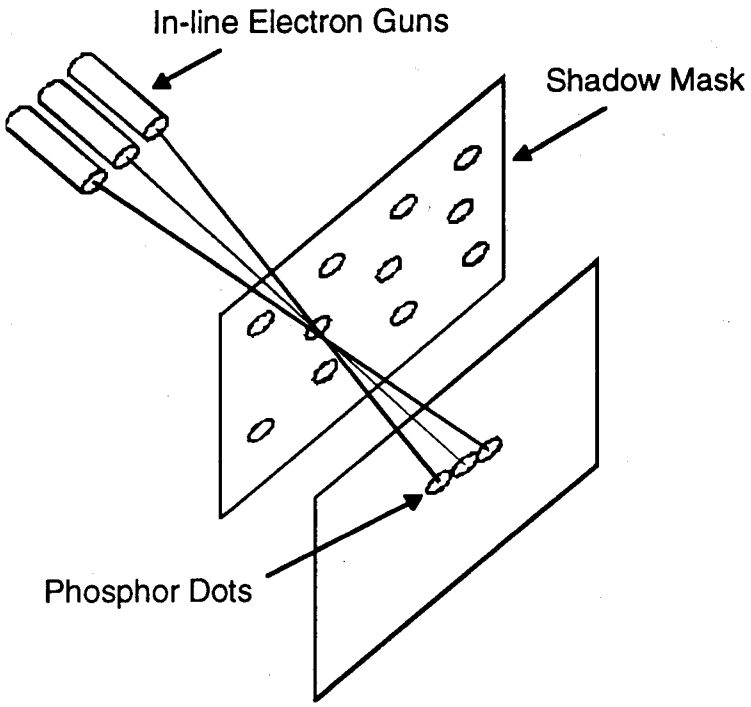

Figure 4. Illustration of an in-line gun CRT.

Figure 5 shows that the phosphor dot structure of an in-line gun CRT. In comparison to delta gun CRTs, the phosphor dots are shifted to align the blue dots with the shadow mask holes. Nevertheless, the geometric relationships for in-line gun phosphor dot structure and shadow mask holes are identical to those of the delta gun CRT; that is, Eqs. 1 and 2 apply to both types of phosphor dot CRT.

II.1.b Phosphor Stripe Displays. The phosphor stripe CRT is illustrated in Figure 6. Phosphor stripe CRTs have some similar features as in-line gun CRTs; that is, electron beams pass through a shadow mask to illuminate phosphor. However, phosphor strip CRTs have shadow-masks constructed with slits rather than holes and have continuous vertical stripes of phosphor instead of discrete phosphor dots. In the phosphor strip CRT, the phosphor structure does not sample the LSF in the vertical

screen dimension.

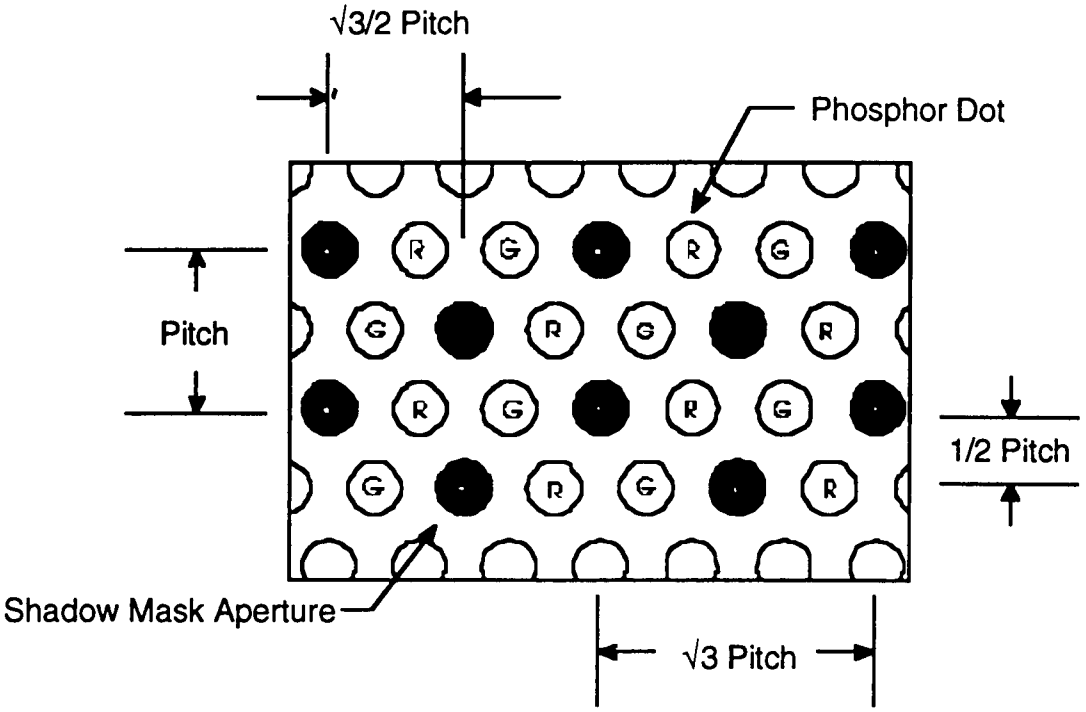

Figure 5. Phosphor dot pattern for in-line gun CRT.

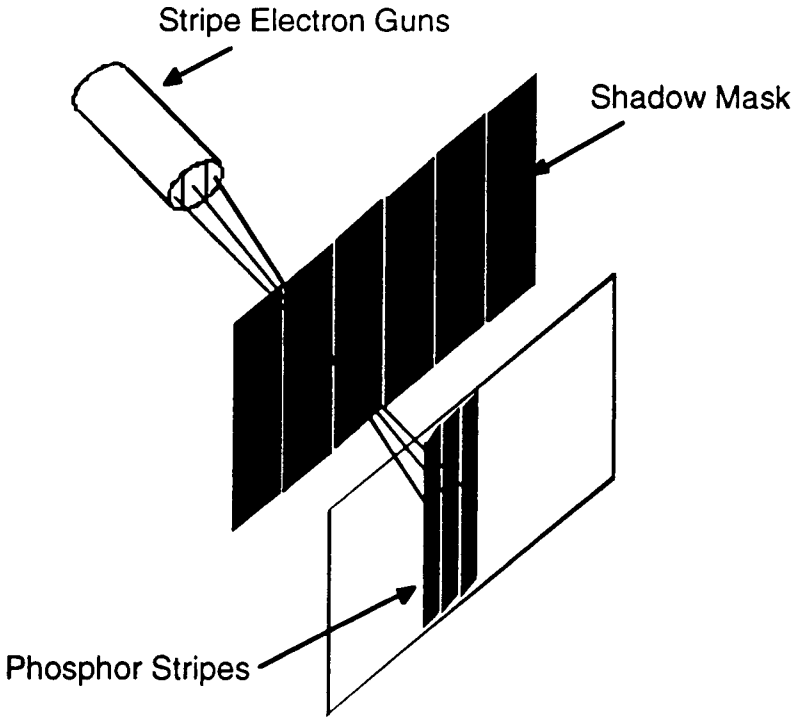

Figure 6. Schematic of phosphor stripe CRT.

The screen geometry of a phosphor stripe CRT is shown in Figure 7. For phosphor stripe CRTs, P is defined along the horizontal screen dimension and it is equal to P_h. In comparison to phosphor dot CRTs with equal P values, P_h is $\sqrt{3}$ times smaller for phosphor strip CRTs as compared with phosphor dot CRTs. In other words, a vertical line presented on a phosphor stripe CRT will be sampled more often in the horizontal dimension than the same line on a phosphor dot CRT.

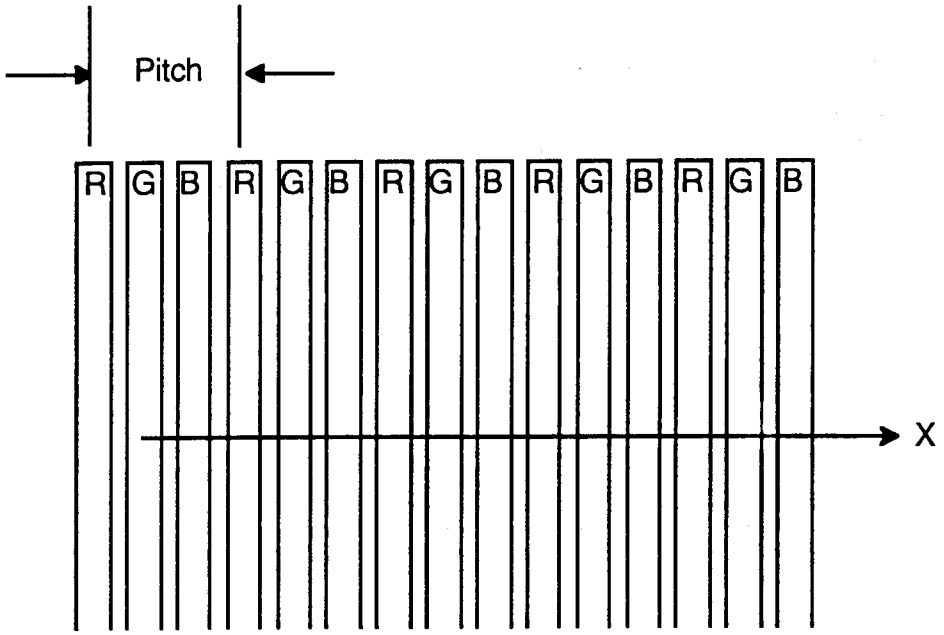

Figure 7. Structure of phosphor stripe color CRT.

II.1.b Screen Display Parameters. Several parameters are required to characterize the image-forming properties of color CRTs (see Table 1). These parameters account for the spatial dimensions of the phosphor dots and stripes, as well as the size and placement of the electron beam profiles.

In most color CRTs, the red, green, and blue phosphor dots or stripes are the same size. However, for the analysis purposes, the size of the phosphor dots (stripes) were defined separately to allow the procedures to examine different phosphor dot (stripe) dimensions. The radii of the red, green, and blue phosphor dots are denoted as r_r, r_g, and r_b, respectively; whereas, the width of the red, green, and blue phosphor stripes are denoted as s_r, s_g, and s_b, respectively.

The Line Spread Function (LSF) of an electro-optical display is the luminance distribution across the width of a line (or pixel) on the screen. The size of the LSF

determines the smallest discernible detail in an image. In the present report, the LSF is treated as a one-dimensional function that extends along the horizontal dimension of the screen. For monochrome CRTs, the LSF is a continuous Gaussian-shaped luminance distribution. For color CRTs, the LSF is a complex distribution, because the electron beams from each gun are sampled by the shadow mask and phosphor structure, and because the multiple electron beams must overlap one another to form a composite LSF.

Table 1. Color CRT Screen Parameters

Parameter	Description
Y	LSF-to-Dot (LSF-to-Stripe) Phase
f_b	Blue-to-Green Misconvergence
f_r	Red-to-Green Misconvergence
I_b	Peak intensity of blue LSF
I_g	Peak intensity of green LSF
I_r	Peak intensity of red LSF
P	Pitch of the shadow mask
P_h	Horizontal pitch of phosphor dots (stripes)
P_v	Vertical pitch of phosphor dots
LSF	Line Spread Function
PMLSF	Pre-Mask Line Spread Function
$PMLSF_r$	Red Pre-Mask Line Spread Function
$PMLSF_g$	Green Pre-Mask Line Spread Function
$PMLSF_b$	Blue Pre-Mask Line Spread Function
r_b (s_b)	Radius (width) of blue phosphor dots (stripes)
r_g (s_g)	Radius (width) of green phosphor dots (stripes)
r_r (s_r)	Radius (width) of red phosphor dots (stripes)
w_b	Full-width at half-maximum intensity of blue line
w_g	Full-width at half-maximum intensity of green line
w_r	Full-width at half-maximum intensity of red line

In this report, we introduce the notion of the Pre-Mask Line Spread Function (PMLSF) to describe the color CRT LSF prior to the spatial sampling by the shadow mask and phosphor structure. There is a PMLSF for each color CRT electron gun; typically, red PMLSF ($PMLSF_r$), green PMLSF ($PMLSF_g$), and blue PMLSF ($PMLSF_b$). The peak

luminance of the $PMLSF_r$, $PMLSF_g$, and $PMLSF_b$ are denoted as l_r, l_g, and l_b, respectively. And, the full-width at one-half peak luminance of the $PMLSF_r$, $PMLSF_g$, and $PMLSF_b$ are denoted as w_r, w_g, and w_b, respectively.

Two spatial phase relationships affect the images rendered on color CRT screens. The first phase relationship involves the placement of the composite LSF on the phosphor dot structure, and it is called the LSF-to-Dot Phase (for phosphor dot CRTs) or LSF-to-Stripe Phase (for phosphor stripe CRTs). The phase relationship is defined as the distance between the $PMLSF_g$ peak intensity point and the center of the closest green phosphor dot.

The second phase relationship involves the misconvergence among the three PMLSFs. For color CRTs employing three electron guns, the misconvergence phase is described by two parameters: Blue misconvergence (f_b), which is the distance between the $PMLSF_g$ and $PMLSF_b$ peak intensity points, and Red misconvergence (f_r), which is the distance between the $PMLSF_g$ and $PMLSF_r$ peak intensity points.

II.2 Image Quality Metrics

This section presents an overview of the image quality metrics used in the visual display community. For a detailed review of these metrics, the reader is referred to Beaton and Farley (1991).

Image quality is the key concept underlying many engineering decisions made during the design of visual display systems. The concept of image quality refers to the amount of task-appropriate information presented to an observer from viewable regions of a display screen. From an engineering standpoint, several physical characteristics of a display system limit the levels of achievable image quality, such as bandwidth, resolution, addressability, color gamut, and luminance contrast.

The relationships among physical display characteristics and perceived image quality are complex. For example, perceived image quality can increase faster with increasing display bandwidth at low luminance contrast levels as compared to high luminance contrast levels (Beaton, 1986). Many of the perceptual relationships among physical display characteristics and perceived image quality levels have been studied over the past 50 years. The display design principles derived from these studies have been captured in quantitative measures or so-called "metrics" of image quality (see, for reviews, Beaton, 1984; Snyder, 1985).

Most image quality metrics are based on spatial frequency-domain representations of the display device and the human observer. Specifically, the capacity of a display system to transmit a signal is indexed by the Modulation Transfer Function (MTF). The MTF expresses the relative amount of modulation (i.e., normalized luminance contrast) produced by a display system as a function of spatial frequency. For all realizable display systems, the MTF decreases with increasing spatial frequency, and, thus, all displays possess a finite capacity (bandwidth) to transmit information signals (Snyder, 1980).

While the MTF expresses the capacity of a display system to transmit signals, a similar spatial frequency-domain function indexes the capacity of human observers to perceive those signals. The Contrast Threshold Function (CTF) expresses the amount of modulation required by the human visual system to detect the spatial frequency components of an image. Each CTF value represents the minimum amount of

modulation required by the human visual system to detect a particular spatial frequency component. Various psychophysical procedures can be used to manipulate the probability of detection; however, the 50% probability level is used most often. In general, the CTF increases with increasing spatial frequency; however, the CTF magnitudes are affected by viewing conditions. Nevertheless, the general shape of the CTF indicates that the human visual system has finite capacity to detect spatial frequency components of image signals (Snyder, 1980).

The MTF and CTF describe fundamental aspects of the concept of image quality; that is, the MTF quantifies the amount of signal modulation available from a display system, whereas the CTF quantifies the amount of signal modulation required by a human observer. Using these two quantitative functions, numerous unitary metrics of image quality have been formulated to help engineers account for the perceptual tradeoffs associated with decisions regarding competing display design concepts.

Among the available image quality metrics, the best-known one is the Modulation Transfer Function Area (MTFA) metric (Borough, Fallis, Warnock, and Britt, 1967; Snyder, 1973). The MTFA metric is defined as:

$$MTFA = \int_{v_l}^{v_u} MTF(\omega)\text{-}CTF(\omega).d\omega, \qquad \text{(Eq. 3)}$$

in which

MTF is the Modulation Transfer Function,

CTF is the Contrast Sensitivity Function,

v_l is the lower limit of integration,

v_u is the upper limit of integration, and

ω is spatial frequency in cycles per unit visual angle.

The MTFA metric is a single number index of the total amount of visually detectable signal modulation presented by a display system across its spatial frequency passband. The MTFA metric has enjoyed a history of use in the photographic and optical imaging industries. It also has been adopted as the *de facto* standard metric in the computer displays industry (ANSI/HFS 100-1988).

Despite its acceptance within the visual display community, the MTFA metric is not a flawless predictor of image quality under all display viewing conditions. Indeed, workers in this arena have recognized several limitations of the MTFA metric and have sought to develop improved image quality metrics (Beaton, 1984).

One limitation of the MTFA metric is its low numerical sensitivity to subtle changes in the CTF, such as those caused by changes in observer's luminance adaptation level or image noise levels. The low sensitivity of the MTFA metric to shifts of the CTF stems from the fact that MTF magnitudes typically are large in comparison to CTF magnitudes, particularly at lower spatial frequency values (*i.e.*, less than 10 cycles per degree of visual angle). In other words, the subtraction of small CTF values from larger MTF values often does not produce substantial changes in MTFA values.

The Integrated Contrast Sensitivity (ICS) metric (van Meeteren, 1973) affords greater sensitivity to subtle changes in the CTF as compared to the MTFA metric. The ICS metric is defined as

$$ICS = \int_{v_l}^{v_u} \frac{MTF(\omega)}{CTF(\omega)} . d\omega, \qquad \text{(Eq. 4)}$$

in which the symbol definitions are identical to Eq. 3.

The analytical form of the ICS metric embodies the operation of "cascading" component transfer functions from linear systems theory. That is, the MTF is point-by-point multiplied with the inverse CTF. The inverse CTF has been interpreted by visual science researchers as the transfer function of the human visual system. The inverse CTF is referred to as the Contrast Sensitivity Function (CSF). Since the ICS metric integrand is the product of the MTF and inverse CTF, ICS values can change rapidly with subtle changes in CTF and MTF values (Beaton, 1984).

A theoretical limitation of the ICS metric (and MTFA metric as well) is that modulation levels are weighted uniformly across the spatial frequency passband. In the metric formulation, a unit of modulation at a low spatial frequency influences the metric value by the same amount as a unit of modulation at a high spatial frequency. Several workers in this field, however, have noted that the contribution of modulation to

perceived image quality levels varies nonuniformly across the spatial frequency passband (Carlson, 1982, Carlson and Cohen, 1980).

The Square-Root Integral (SQRI) metric (Barten, 1987, 1988, 1989a, 1989b, 1989c, 1990a, 1990b 1991) is based on a non-linear scaling of modulation across spatial frequencies. The SQRI metric is defined as:

$$SQRI = \frac{1}{\ln 2} \int_{v_l}^{v_u} \sqrt{\frac{MTF(\omega)}{CTF(\omega)}} . d\omega, \qquad \text{(Eq. 5)}$$

in which all symbol definitions are identical to Eq. 3.

The SQRI metric scales visually-weighted modulation levels by two operations: (1) a square root operator, and (2) a logarithmic integration. These analytic operations emphasize the contributions of lower modulation levels at lower spatial frequencies in the SQRI metric value. Purportedly, the compressive scaling performed by the SQRI metric matches observed patterns in human suprathreshold contrast discriminations. The SQRI metric is claimed to provide an improved index of image quality effects associated with physical display parameters in comparison to the MTFA and ICS metrics.

II.3 Purpose of Project

It is beyond the present scope of work to evaluate and compare the above mentioned image quality metrics. Rather, the intent here is to note that imaging capacity of display systems, as described by the MTF, is common to all of the image quality metrics reviewed. It is likely that future image quality metrics will continue to use the MTF as a component term.

The purpose of the present work is to investigate the effects of sampling artifacts in color CRT displays on the MTF. Procedures for determining and using the MTF of a color CRT display are presented.

Section III. Image Quality of Sampled Displays

This section describes an approach for evaluating spatially sampled displays with MTF-based metrics of image quality. The notions of sampling criteria and the aliasing for color CRTs are discussed.

III.1 Nyquist Sampling Criterion

For the purpose of determining the image quality of color CRTs, it is important to note that the LSF is sampled spatially by the phosphor structure; that is, by the discrete phosphor dots or stripes. From the Nyquist sampling theorem (Nyquist, 1928), the highest spatial frequency that can be represented accurately in the MTF derived from a color CRT LSF is given by:

$$f_{max} = \frac{1}{2S}, \qquad \text{(Eq. 6)}$$

in which

S is the distance between the same-colored phosphor dots or stripes and

f_{max} is the maximum spatial frequency (in units of S^{-1}) .

The Nyquist theorem sets an upper limit on the bandwidth of a transmission system. Frequency components of a signal that occur at and beyond f_{max} can not be transmitted faithfully by the system (Park, 1984). These frequency components are aliased with lower frequency components in the output signal.

For color CRTs, the aliased spatial frequencies appear as "beat" frequencies and moiré patterns on the display screen. Figure 8a shows the luminance pattern of an On-Off pixel pattern displayed on a phosphor stripe CRT. It is evident in Figure 8a that the output signal contains low spatial frequency aliasing. The aliased frequency components are not part on the signal; rather, they stem from sampling artifacts of the display device.

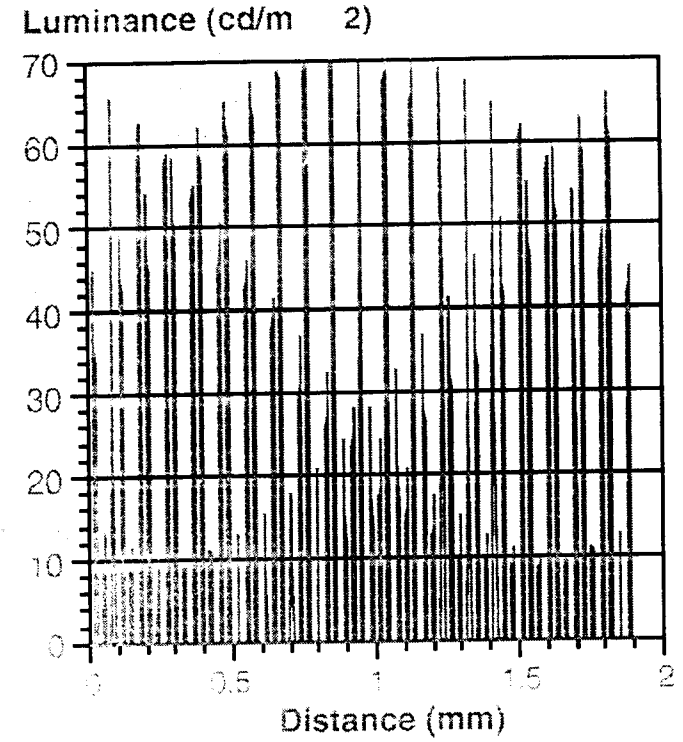

(a)

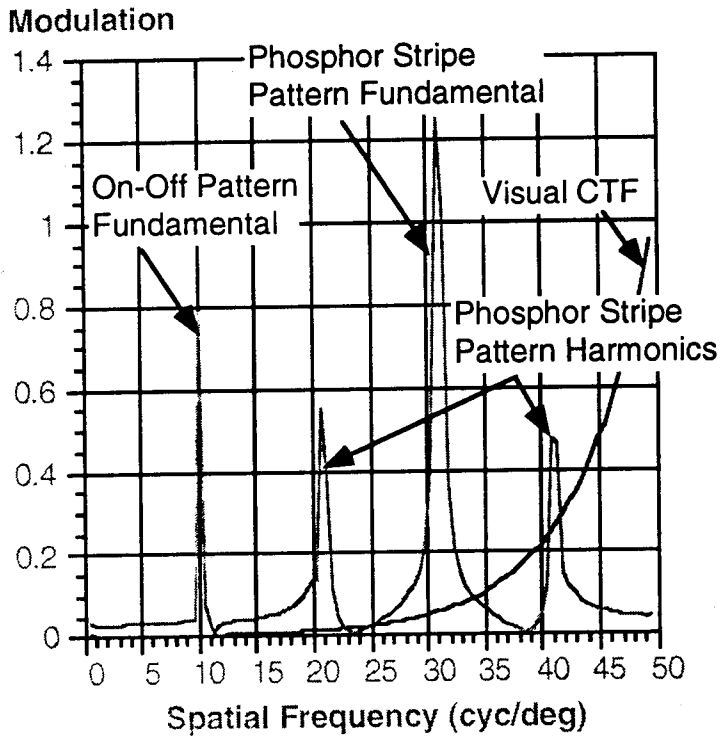

(b)

Figure 8. Luminance distribution of On-Off pixel pattern (A) and its associated spatial frequency modulation spectrum (B) on a phosphor stripe CRT. (screen diagonal = 15 in; P = 0.31 mm; viewing distance = 550 mm).

Figure 8b shows the spatial frequency modulation spectrum of the On-Off pixel pattern. The fundamental frequency of the actual signal is represented by the modulation peak at about 10 cycles per degree of visual angle (for an observer viewing distance of 550 mm). The modulation peaks occurring at about 21, 31, and 41 cycles per degree corresponds to the periodicity of the red, green, and blue phosphor stripes. Since the alias frequencies are not present in the input to the display, they distort the output of the display.

III.2 STAV Criterion

To describe the amount of visually detectable modulation due to alias frequencies, the Super-Threshold Alias Value (STAV) is defined as:

$$STAV = AL(\omega) - CTF(\omega) \qquad \text{(Eq. 7)}$$

in which

$AL(\omega)$ is the modulation of alias spatial frequency ω and
$CTF(\omega)$ is the Contrast Threshold Function value at spatial frequency ω.

A STAV less than or equal to zero indicates that there is no detectable modulation at the alias frequency; thus, the input frequency is reproduced without visible interference. As the modulation of the alias frequency increases, the STAV increases. As the STAV exceeds a value of zero, the input frequency becomes increasingly distorted with the alias frequency.

For the purposes of this report, the **STAV Criterion** is defined as:

> *If the STAV at a spatial frequency exceeds zero, then the spatial frequency component does not provide undistorted information to the observer. Therefore, that spatial frequency is not used in the MTF-based metric computations.*

Because the upper limit of integration (*i.e.*, v_u in Eq. 3-5) is critical for computing the image quality metrics, the STAV Limit is useful for evaluating the image quality of spatially sampled display systems.

The method for computing MTF-based image quality metrics for sampled displays begins with LSF data obtained by measuring or computing the luminance profile across the width of a one pixel-wide line. The LSF then is converted into the spatial frequency domain by a forward Fourier transform and scaled (normalized) to give the MTF in appropriate amplitude (modulation) units. The MTF is used in the MTFA, ICS, and SQRI expressions, as defined by Eqs. 3-5. The upper and lower limits of integration must be set in these equations, and the metrics must be calculated over the same spatial frequency range to yield comparable values.

For a continuous display devices, such as photographs or vector-scanned monochrome CRTs, the upper limit of integration for the MTFA is set to the crossover spatial frequency; that is, the point where the MTF amplitude equals and the CTF amplitude (see Figure 9). The upper limits of integration for the ICS and SQRI metrics are set at the lower of the Nyquist spatial frequency or the spatial frequency where the CTF amplitude equals unity (*i.e.*, about 45-55 cycles per degree of visual angle).

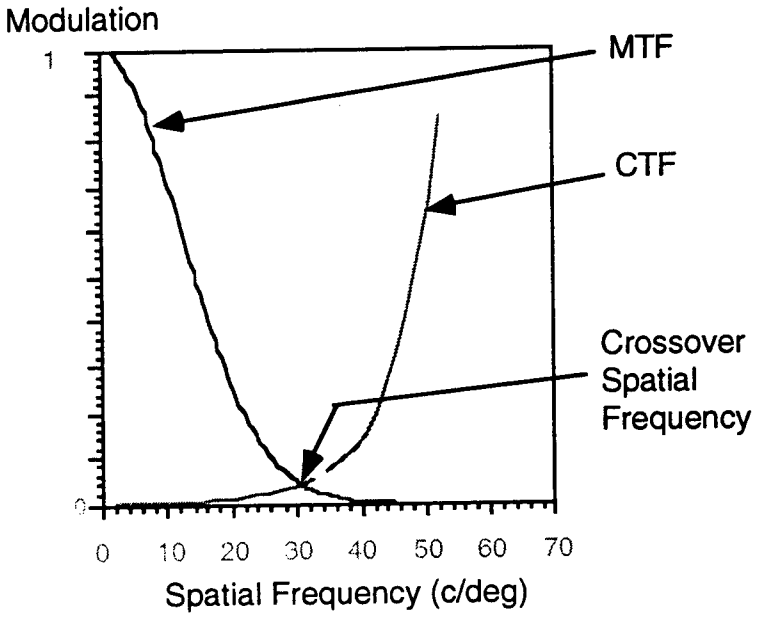

Figure 9. Crossover spatial frequency in MTFA metric.

For spatially sampled display devices, the STAV Criterion must be used. That is, the STAV is computed for the highest spatial frequency in the MTF. If the STAV Criterion is met, then that spatial frequency sets the upper limit of integration. If the Sampling

Criterion is not met, the STAV for the next lower spatial frequency is computed (*i.e.*, two pixels on/two pixels off pattern). The process of sequentially lowering the spatial frequency point is repeated until the STAV Criterion is met. When the STAV Criterion is met, the spatial frequency is used for the upper limit of integration for the ICS and SQRI metrics. The upper limit of integration for the MTFA metric is the lower of the spatial frequencies associated with the STAV Criterion and the MTFA crossover point.

Section IV. Investigation

Since the STAV influences the image quality calculations, it is important to understand how its value is affected by display device and measurement system parameters. This section explores the effect of phosphor dot or stripe pitch, dot or stripe width, number of horizontal pixels, Resolution to Addressability Ratio (RAR), adaptive luminance, and measurement aperture height and width on the STAV.

IV.1 Method

A computer model was used to generate the data for the analysis of STAV values (Appendix A). The computer program consists of a CRT model, a measurement model, and a function to compute the STAV from the simulated measurement data. The computer model creates a two-dimensional luminance profile of the image-forming surface of a color CRT, according to a list of display device and measurement system parameters. A simulated one-dimensional photometric scan then is created by using the two-dimensional luminance data. The STAV and image quality metrics are computed from the simulated scan data.

The investigation of STAV was conducted for the green component of a color CRT image. Since the red, green, and blue image components differ only in amplitude, the STAV changes by less than one percent across these colors. The STAV for more than one primary color, such as white, are lower than the single-color STAV. Thus, the green STAV represents a worst-case condition.

IV.1.a Model Parameters. Several color CRT and measurement system parameters were used in the analytical investigation. These parameters were chosen to reflect the current state of color CRT display technologies. Where appropriate, the range of parameter values was expanded beyond current technology limits to study the increase or reduction of the STAV. The model parameters are discussed below.

Display size, viewing distance, and the phosphor intensities were held constant. A display size of 381 mm (15 inch) diagonal was used, because it is a popular mid-range CRT size. Viewing distance was set to 550 mm (21.7 inches) since this is a common viewing distance for the selected display size. To set the phosphor intensities, several color CRT displays were measured to determine the ratio of red,

green, and blue phosphor luminances. When normalized to 100 cd/m^2, the color CRTs examined yielded about 21 cd/m^2 for the red phosphor, 70 cd/m^2 for the green phosphor, and 9 cd/m^2 for the blue phosphor. These luminance values were used for the STAV computations.

Three values of phosphor dot pitch were varied in the STAV calculations: 0.31 mm, 0.26 mm, and 0.21 mm. These values represent a dot pitch range often found in commercial phosphor dot CRT displays. It is unlikely that a pitch of larger than 0.31 mm would be used in a 381 mm (15 inch) diagonal CRT. Likewise, a pitch smaller than 0.21 mm is not practical, because the display would be too expensive for most commercial applications.

The phosphor dot diameter is expressed as a percentage of the largest possible dot diameter. For a given pitch, a phosphor dot cannot overlap another dot. Therefore, the maximum dot diameter is one third the distance between adjacent phosphor dots of the same color (P_h). Three dot diameters were used in the STAV calculations: 20, 40, and 60 percent of the maximum dot diameter. Table 2 shows the dot diameters (in mm) as a function of phosphor dot pitch and diameter.

Table 2. Phosphor Dot Diameters (in mm) as a Function of Phosphor Dot Pitch

	Percent of Maximum		
Pitch	20	40	60
0.31	0.0358	0.0716	0.1074
0.26	0.0300	0.0600	0.0901
0.21	0.0242	0.0485	0.0727

The number of horizontal pixels also was varied across three levels: 640, 1024, and 1280. These levels represent the number of horizontal pixels addressed in most contemporary desktop color displays.

The RAR is the ratio of pixel width (*i.e.*, full width at 50% peak luminance) to pixel addressability (*i.e.*, distance between adjacent pixels). Four levels of RAR were used in the STAV calculations: 0.75, 1.0, 1.25, and 1.5. An RAR greater than unity is common for phosphor dot CRTs. Table 3 shows the spot width (in mm) as a function of

RAR and addressability.

Table 3. Spot Size (mm) as a Function of RAR and Addressability

	Addressability		
RAR	640	1024	1280
0.75	0.353	0.220	0.176
1.00	0.470	0.294	0.235
1.25	0.588	0.367	0.294
1.50	0.705	0.441	0.353

Two adapting luminance were used in the STAV calculation: 50 cd/m^2 and 100 cd/m^2. Adapting luminance affects the STAV by shifting the CTF; however. large differences in adapting luminance are required to shift the CTF substantially. The two values selected represent low and high adaptive luminance values for CRT viewing conditions, but not necessarily for substantial CTF changes.

Several parameters of a photometric measurement also were varied in the analytical work. Specifically, the measurement aperture width and height were defined as a percentage of the CRT spot width. The three aperture width values were used: 2, 6, and 12 percent. The 12 percent value is suggested by the visual display industry (see, ANSI/HFS 100-1988), whereas the 2 percent value allows a maximum numerical accuracy in the calculations. Three aperture height values were used in the STAV calculations: 200, 400, and 800 percent. The aperture height values are used commonly in scanning-slit and linear-array detector systems.

Table 4 lists the parameter ranges used for the phosphor dot CRT STAV investigation. These parameters also were used for the phosphor stripe color CRT investigation, with two exceptions: aperture height and phosphor dot diameter. Since a phosphor stripe is uniform in the vertical direction (along the stripe axis), aperture height has no effect on the measurements. Therefore, the aperture height parameter was not included in the phosphor stripe CRT evaluation. However, the phosphor stripe width replaced the dot diameter parameter. Phosphor stripe width was expressed as a percentage of the maximum possible stripe width, and the values of 40, 60, and 80 percent were selected. Table 5 shows the stripe width (in mm) as a function of pitch and percent

maximum width.

Table 4. Parameters of STAV Evaluation for Phosphor Dot Color CRTs

Parameter	Range
Pitch	0.31, 0.26, 0.21 mm
Number of Pixels	640, 1024, 1280 pixels
RAR	0.75, 1.0, 1.25, 1.5
Percent Maximum Dot Diameter	20%, 40%, 60%
Adaptive Luminance	50, 100 cd/m^2
Aperture Width (Percent Spot Width)	2%, 6%, 12%
Aperture Height (Percent Spot Width)	200%, 400%, 800%

Table 5. Phosphor Stripe Width (in mm) as a Function of Pitch and Percent of Maximum

	Percent of Maximum		
Pitch	40	60	80
0.31	0.0413	0.0620	0.0827
0.26	0.0347	0.0520	0.0693
0.21	0.0280	0.0420	0.0560

Table 6 summarizes the parameters used in the STAV evaluation for phosphor stripe color CRT displays.

Table 6. Parameters of STAV Evaluation for Phosphor Stripe Color CRTs

Parameter	Range
Pitch	0.31, 0.26, 0.21 mm
Number of Pixels	640, 1024, 1280 pixels
RAR	0.75, 1.0, 1.25, 1.5
Percent Maximum Stripe Width	40%, 60%, 80%
Adaptive Luminance	50, 100 cd/m2
Aperture Width (percent Stripe Width)	2%, 6%, 12%

IV.2 Results

The STAVs were analyzed separately for the phosphor dot and strips CRTs, although the analysis procedures were identical. For each type of CRT, the STAVs were subjected to first-order regression and Analyses of Variance (ANOVA) procedures to determine how parameters affected the computed values.

IV.2.a Phosphor Dot Displays. An eight-term (*i.e.*, all model parameters, plus an intercept term), first-order linear regression was computed for the phosphor dot CRT STAVs. Table 7 presents a summary of the regression analysis. The regression model accounted for 78% of the variance (r = 0.881). This finding suggests that STAV changes in a nearly linear fashion with variations in some of the model parameters.

Table 7. Regression Summary for Phosphor Dot CRT STAV Data

Count:	1944				
r:	0.881				
r^2:	0.777				
Adjusted r^2:	0.776				
RMS Residual:	0.13				
	df	**S S**	**M S**	**F**	***p***
Model	7	113.255	16.179	963.16	0.0001
Error	1936	32.521	0.017		
Total	1943	145.776			

To determine which parameters affected the STAVs, a seven factor ANOVA was computed. As shown in Table 8, the effects of Adaptive Luminance, Phosphor Dot Diameter, Number of Pixels, RAR, and Pitch were significant ($p < 0.0001$). These effects are discussed below. However, the data trends show that the STAV increases with increasing Adaptive Luminance, Number of Pixels, and Pitch, and it decreases with increasing RAR and Phosphor Dot Diameter.

Table 8. ANOVA Summary for Phosphor Dot CRT STAV Data

Source	df	S S	M S	F	*p*
Adaptive Luminance	1	1.514	1.514	90.116	0.0001
Aperture Height	1	1.05E-06	1.05E-06	6.23E-05	0.9937
Aperture Width	1	0.029	0.029	1.711	0.1910
Phosphor Dot Diameter	1	0.583	0.583	34.708	0.0001
Number of Pixels	1	0.880	0.880	52.398	0.0001
RAR	1	20.176	20.176	1201.067	0.0001
Pitch	1	90.073	90.073	5362.117	0.0001
Residual	1936	35.521	0.017		

IV.2.b Phosphor Stripe Displays. A seven-term (*i.e.*, all model parameters, plus an intercept term), first-order linear regression was computed for the phosphor stripe CRT STAVs. Table 9 presents a summary of the regression analysis. The regression model accounted for 71% of the variance (r = 0.841). This finding suggests that STAV changes in a nearly linear fashion with variations in some of the model parameters.

Table 9. Regression Summary for Phosphor Stripe CRT STAV Data

Count:	648
r:	0.841
r^2:	0.708
Adjusted r^2:	0.705
RMS Residual:	0.086

	df	S S	M S	F-Value	*p*
Model	7	11.52	1.919	258.634	0.0001
Error	1936	4.755	0.007		
Total	1943	16.268			

Table 10 presents the ANOVA findings, which indicate that the effects of Adaptive

Luminance, RAR, and Pitch were significant ($p<0.0001$). The data trend across these effects indicated the STAV increases with increasing Adaptive Luminance, Number of Pixels, and Pitch, whereas the STAV decreases with increasing RAR.

Table 10. ANOVA Summary Table for Phosphor Stripe CRT STAV Data

Source	df	S S	M S	F-Value	*p*
Adaptive Luminance	1	0.603	0.603	81.236	0.0001
Aperture Width	1	4.87E-05	4.87E-05	0.007	0.9354
Phosphor Stripe Width	1	0.012	0.012	1.566	0.2112
Number of Pixels	1	0.009	0.009	1.269	0.2605
RAR	1	1.251	1.251	168.673	0.0001
Pitch	1	9.637	9.637	1299.056	0.0001
Residual	641	4.755	0.007		

In general, the ANOVA results show that aperture width and height do not effect the STAV. This finding most likely stems from the limited range examined for these parameters. Moreover, the ANOVA findings indicate that phosphor stripe width and number of pixels do not effect the STAV. One explanation for this finding is that modulation values of on-off line patterns on phosphor stripe CRTs often exceed unity. However, modulation values were not allowed to exceed unity in the STAV calculation. Thus, the computational procedures may have eliminated these parameter effects.

IV.2.c Illustration of Effects. While the statistical findings above are helpful in understanding the STAV behavior, it also is instructive to examine the On-Off patterns and their modulation spectra. Figures 10-13 show these data for phosphor dot CRTs varying in pitch. The display and measurement system parameters used are listed in Table 11.

Table 11. Model Parameters for Pitch Analysis

Parameter	Value
Pitch	0.31, 0.26, 0.21, 0.11 mm
Number of Pixels	1024 (horizontal)
RAR	1.0
Dot Diameter	60% of maximum diameter
Screen Size	381 mm diagonal
Viewing Distance	550 mm (21.65 inches)
Aperture Width	2% of the spot width
Aperture Height	400% of the spot width

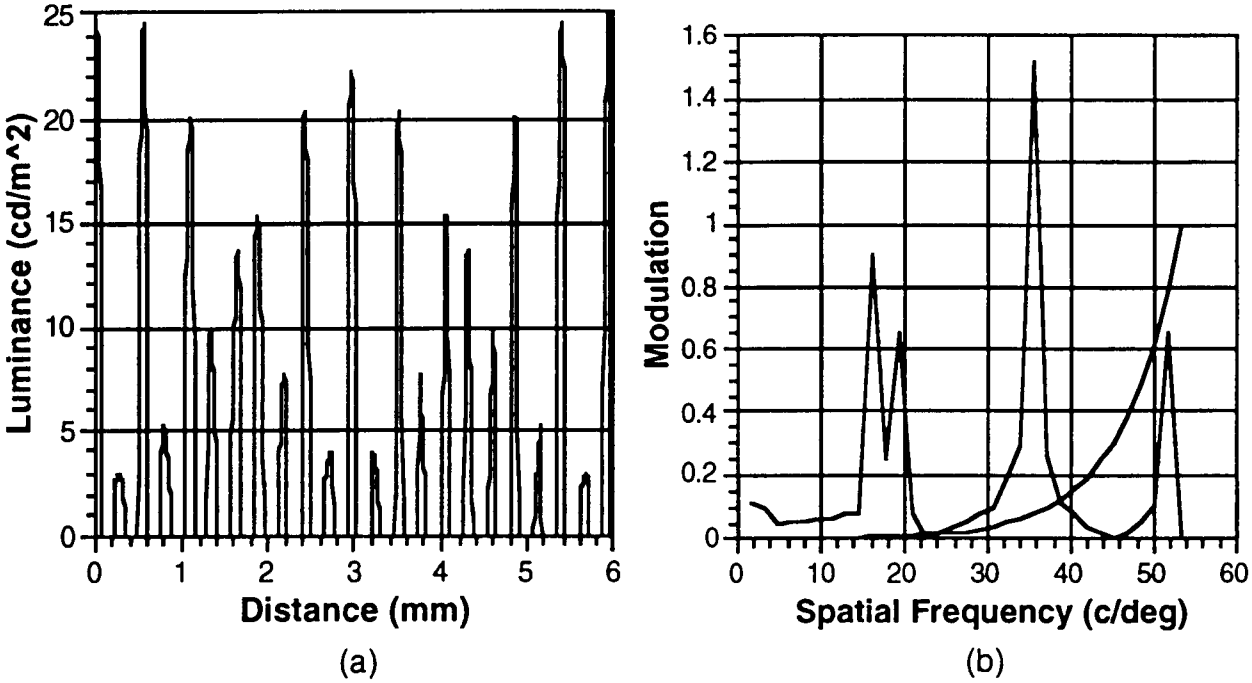

Figure 10. On-Off pattern (a) and associated modulation spectrum (b) for phosphor dot CRT (Pitch = 0.31; STAV = 0.9215).

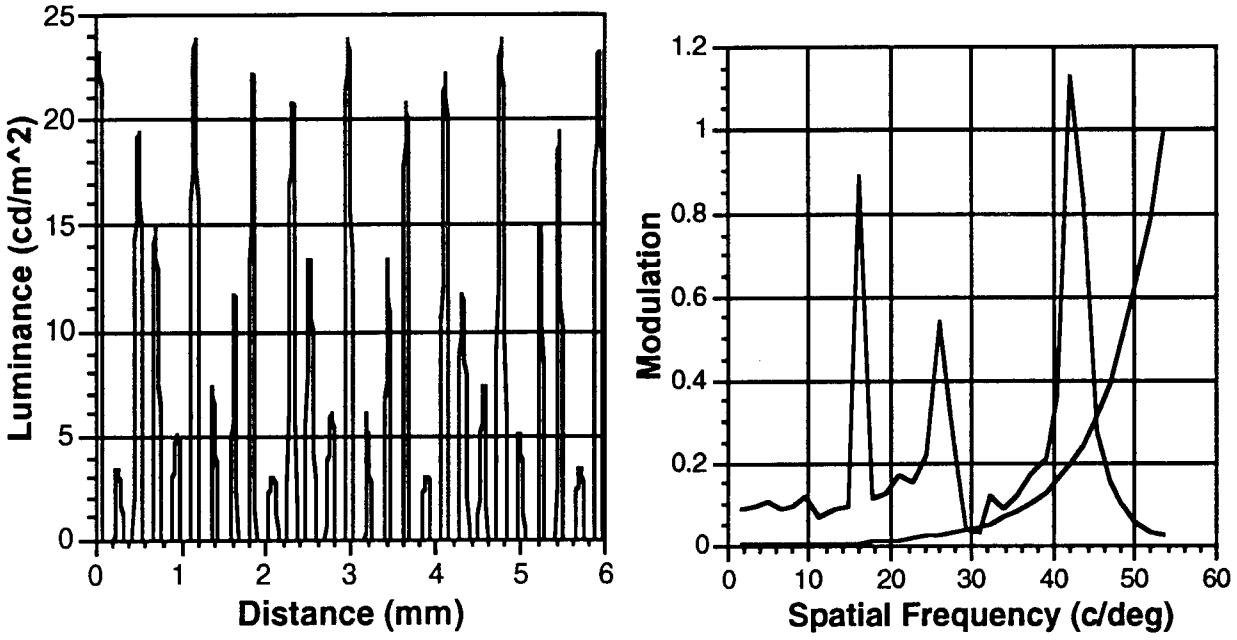

(a) (b)

Figure 11. On-Off pattern (a) and associated modulation spectrum (b) for phosphor dot CRT (Pitch = 0.26; STAV = 0.8059).

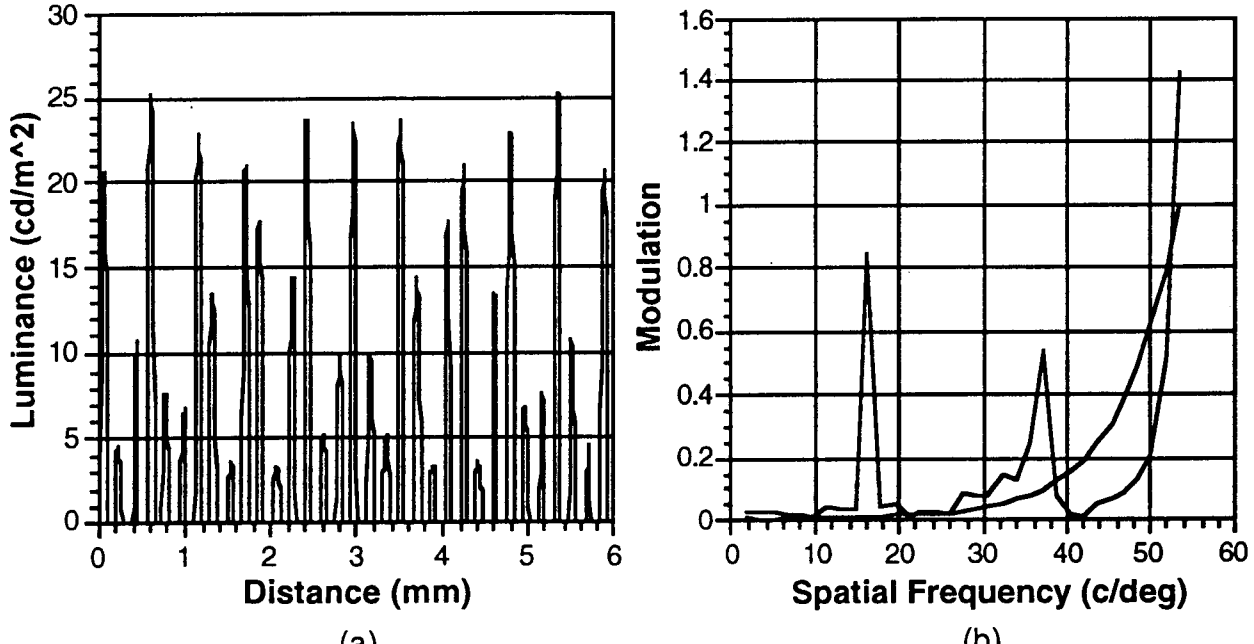

(a) (b)

Figure 12. On-Off pattern (a) and associated modulation spectrum (b) for phosphor dot CRT (Pitch = 0.21; STAV = 0.4442).

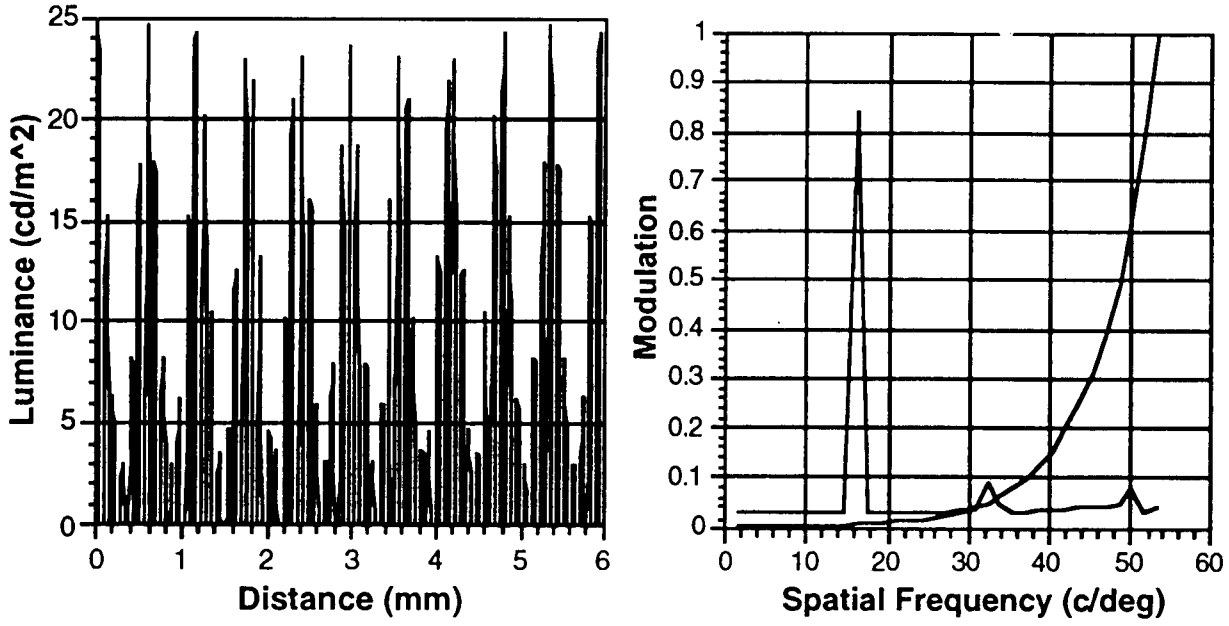

Figure 13. On-Off pattern (a) and associated modulation spectrum (b) for phosphor dot CRT (Pitch = 0.11; STAV = 0.0438).

Because the number of pixels was constant across the CRTs shown in Figures 10-13, the spatial frequency of the On-Off pattern also is constant at 16.12 cycles per degree. The first peak in the modulation spectra reflect this component of the On-Off patterns. Moreover, the phosphor pitch values of 0.31, 0.26, 0.21, and 0.11 mm have fundamental spatial frequencies of 37.76, 42.63, 52.78, and 100.77 cycles per degree, respectively. For the 0.31 and 0.26 mm pitch displays (Figures 10 and 11), the fundamental frequency of the phosphor pitch has the largest modulation and it does not meet the STAV Criterion. For the 0.21 mm pitch display (Figure 12), the phosphor pitch peak occurs near the limit of vision (*i.e.,* about 50 cycles per degree), but it also fails to meet the STAV criterion. The 0.11 mm pitch display (Figure 13) meets the STAV Criterion, because the phosphor pitch modulation at 100.77 cycles per degree occurs beyond the limit of vision.

Figure 10 shows the effects of sampling by the phosphor dot pattern. Since the 0.31 mm pitch sampling frequency is low, artifacts are produced in the On-Off pattern. Indeed, it is difficult to distinguish the On-Off pattern in Figure 10-a. Figure 10-b shows that a phosphor dot harmonic frequency occurs at 19.35 cycles per degree, which is close to the fundamental of the On-Off pattern. Thus, the 0.31 mm pitch is visible and

its sampling frequency causes visible artifacts the On-Off pattern frequency.

Careful examination of Figure 11b-13b shows the effects of increasing phosphor dot sampling frequency. For the 0.26 mm pitch (Figure 11-b), the phosphor pitch peak is 42.63 cycles per degree and the subharmonic peak has relatively low modulation. These effects render the sampling artifacts more difficult to perceive in comparison with those produced by the 0.31 mm pitch. For the 0.21 mm pitch (Figure 12-b), the sampling artifacts are reduced further as compared to the larger pitch displays. The phosphor pitch peak and its subharmonic peak are difficult to detect, because they lie close to the CTF. For the 0.11 mm pitch (Figure 13-b), the On-Off pattern is readily detected since the sampling artifacts are below the CTF.

IV.2.d Misconvergence Effects. To determine the image quality of a color CRT display, one first uses the STAV Criterion to determine the highest spatial frequency that contains undistorted information. Once the upper frequency limit is established, the LSF for the component colors (*i.e.*, red, green, and blue phosphors) are measured. The phase relationship among the LSFs must be maintained at a constant value. This requirement means that the measurements must be made by the same instrument in the same screen location. The peaks of the LSFs can be fit by Gaussian functions to give the Red, Green, and Blue PMLSFs. The image quality metric can be computed from the component PMLSFs or from a composite PMLSF (*i.e.*, sum of the component PMLSFs).

Spot size, number of pixels, glare, adapting luminance, viewing distance, STAV, and misconvergence affect image quality. The effects of spot size, addressability, glare, adapting luminance, and viewing distance have been studied previously (Beaton and Farley, 1991). The effects of STAV and misconvergence on color CRT image quality were studied in this work.

A 381 mm (15 inch) diagonal display with an addressability of 1024 horizontal pixels was chosen as the test display. A viewing distance of 550 mm (21.7 inches) was selected. The RAR was set at 1.0, yielding a spot size of 0.297 mm. PMLSFs were generated with red and blue misconvergence values of -0.297 mm, -0.149 mm, 0.0 mm, 0.149 mm, and 0.297 mm, combined factorially to yield 25 different misconvergence conditions. Appendix B contains plots for these test conditions

The MTFA, ICS, and SQRI were computed for the PMLSF under two conditions: full and reduced addressability. The full addressability condition refers to STAV computations using the entire spatial frequency passband (*i.e.*, STAV Criterion met at highest spatial frequency). The reduced addressability condition refers to STAV computations using one-half of the passband (*i.e.*, STAV Criterion met at second highest spatial frequency). Tables 12 through 15 present the results of these image quality metric computations.

Table 12. MTFA for Red and Blue Misconvergence at Full Addressability (1024 pixels)

			Red (mm)		
Blue (mm)	-0.297	-0.149	0	0.149	0.297
-0.297	9.569433	10.85945	11.34023	10.63216	9.236327
-0.149	10.11039	11.43724	11.93378	11.21408	9.853356
0	10.26271	11.61344	12.2300	11.61344	10.26271
0.149	9.853356	11.21408	11.93378	11.43724	10.11039
0.297	9.236327	10.63216	11.34023	10.85945	9.569433

Table 13. SQRI for Red and Blue Misconvergence at Full Addressability (1024 pixels)

			Red (mm)		
Blue (mm)	-0.297	-0.149	0	0.149	0.297
-0.297	129.5952	131.9684	132.6917	131.4735	128.7322
-0.149	130.6165	132.9748	133.7378	132.5979	130.0496
0	130.8321	133.2465	134.1900	133.2465	130.8321
0.149	130.0496	132.5979	133.7378	132.9748	130.6165
0.297	128.7322	131.4735	132.6917	131.9684	129.5952

Table 14. ICS for Red and Blue Misconvergence at Full Addressability (1024 pixels)

	Red (mm)				
Blue (mm)	-0.297	-0.149	0	0.149	0.297
-0.297	3628.058	3970.964	4084.377	3897.764	3511.361
-0.149	3771.056	4126.636	4250.234	4067.586	3690.381
0	3801.932	4170.207	4325.100	4170.207	3801.932
0.149	3690.381	4067.586	4250.234	4126.636	3771.056
0.297	3511.361	3897.764	4084.377	3970.964	3628.058

Table 15. MTFA for Red and Blue Misconvergence at Reduced Addressability (512 pixels)

	Red (mm)				
Blue (mm)	-0.297	-0.149	0	0.149	0.297
-0.297	6.802	7.088	7.159	7.002	6.646
-0.149	6.919	7.224	7.314	7.174	6.829
0	6.929	7.255	7.371	7.255	6.929
0.149	6.829	7.174	7.314	7.224	6.919
0.297	6.646	7.002	7.159	7.088	6.802

Table 16. SQRI for Red and Blue Misconvergence at Reduced Addressability (512 pixels)

	Red (mm)				
Blue (mm)	-0.297	-0.149	0	0.149	0.297
-0.297	120.24	121.17	121.40	120.89	119.69
-0.149	120.62	121.61	121.89	121.45	120.32
0	120.65	121.71	122.07	121.71	120.65
0.149	120.32	121.45	121.89	121.61	120.62
0.297	119.69	120.89	121.40	121.17	120.24

Table 17. ICS for Red and Blue Misconvergence at Reduced Addressability (512 pixels)

	Red (mm)				
Blue (mm)	-0.297	-0.149	0	0.149	0.297
-0.297	2947.3	3074.6	3105.9	3036	2876.4
-0.149	2999.3	3135.1	3175.2	3112.9	2958.9
0	3003.6	3149.0	3200.5	3149.0	3003.6
0.149	2958.9	3112.9	3175.2	3135.1	2999.3
0.297	2876.4	3036.0	3105.9	3074.6	2947.3

These results demonstrate that misconvergence adversely affects image quality. All metrics show that image quality decreases with increasing misconvergence. The MTFA has a 24.5% reduction from the no misconvergence to worst case misconvergence in the full addressability condition. The worst case misconvergence conditions is when one component PMLSF is at its maximum positive range, and the other one is at its maximum negative range. At the worst case misconvergence condition, the spot is the largest. The affect on the MTF of this larger spot is reduced modulation at the higher spatial frequencies (see Appendix B). The SQRI has a 4.1% reduction from the no misconvergence to worst case misconvergence. The smaller reduction can be attributed to the weighting of the low spatial frequencies in the SQRI metric. A 18.8% reduction is seen in the ICS metric between the no misconvergence case and the worst case misconvergence.

For the reduced addressability condition, the MTFA, SQRI, and ICS showed reductions of 9.84%, 1.95%, and 10.13%, respectively. The reduced effect of misconvergence on image quality stems from the restricted spatial frequency range imposed by the STAV Criterion. In addition, the converged MTFA was reduced from 12.23 to 7.31 between the full and reduced addressability conditions. This reduction is a direct result of the limited spatial frequency range imposed by the STAV Criterion. Reductions of 134.19 to 122.07, and 4325 to 3200, are seen in the SQRI and ICS, respectively, between the full and reduced addressability conditions. Again, the MTFA reduction is the most dramatic because of the importance of the higher spatial frequencies.

Section V. Conclusions

The STAV Criterion may be used to identify the usable spatial frequency range for MTF-based metrics of image quality. the STAV Criterion has the advantages that aliased frequency artifacts are separated from the signal modulation. Thus the STAV Criterion approach provides an understanding of the behavior of image quality effects without the confounding sampling artifacts.

The STAV indexes aliased frequency components as expected. Smaller spots, larger pitch values, decreased number of pixels, and higher adaptive luminance lead to increases in the STAV. Display designers and engineers can employ the STAV to characterize the artifacts produced by color CRTs and other spatially sampled displays (*i.e.*, flat panels).

The pre-mask color CRT metric computations issues resemble those found with continuous screen displays, such as a monochrome CRT. It is important to note that the composite PMLSF may not be Gaussian shaped, because of misconverged component PMLSFs. However, no specialized measurement equipment is required to assessment the color CRT; that is, a two-dimensional detector array is sufficient. It is necessary to use software to fit an analytical function to the component and composite PMLSFs.

The phosphor dot (PDOT) and phosphor stripe (PSTRIPE) computer models proved to be accurate and efficient methods of investigation of image quality issues regarding color CRT displays. These models were used to investigate color CRT displays that are not available commercially. In addition, the speed of the model allowed many color CRT and measurement system parameters to be evaluated.

The scope of this work did not allow an investigation of STAV visibility. It is well known in the human vision literature that contrast thresholds vary with spatial frequency. Therefore, the STAV Criterion should vary with spatial frequency. A visual psychophysical study should be performed to enhance the use of the STAV approach.

Section VII. References

American National Standard for Human Factors Engineering of Visual Display Terminal Workstations. ANSI/HFS 100-1988, Santa Monica: Human Factors Society, 1988.

Barten, P.G.J. The SQRI method: A new method for the evaluation of visible resolution on a display, Proceedings of the Society for Information Display, 28(3), 253-262, 1987.

Barten, P.G.J. Subjective image quality of HDTV pictures. Proceedings of the 9th International Display Research Conference, Japan Display '89 October 16-18, Kyoto, 598-601, 1989(a).

Barten, P.G.J. The effects of picture size and definition on perceived image quality. IEEE Transactions of Electron Devices, 36(9), 1865-1869, 1989(b).

Barten, P.G.J. The square root integral (SQRI): A new metric to describe the effects of various display parameters on perceived image quality. Proceedings of the Society for Photographic Instrumentation Engineers, Human Vision, Visual Processing, and Digital Display, Los Angeles, 1077, 73-82, 1989(c).

Barten, P.G.J. Evaluation of CRT displays with the SQRI method. Proceedings of the Society for Information Display Engineers, 30, 9-14, 1989(d).

Barten, P.G.J. The effects of glass transmission on the subjective image quality of CRT pictures. Proceedings of the 10th International Display Research Conference, EURODISPLAY'90, Amsterdam, The Netherlands, 336-339, 1990(a).

Barten, P.G.J. Evaluation of subjective image quality with the square-root integral method. Journal of the Optical Society of America (A), 7, 2024-2031, 1990(b).

Barten, P.G.J. Evaluation of the effect of noise on subjective image quality. Proceedings of the Society for Photographic Instrumentation Engineers, Unpublished manuscript, 1991.

Beaton, R.J. A human-performance based evaluation of quality metrics for hard-copy

and soft-copy digital imaging systems. Unpublished doctoral dissertation, Virginia Polytechnic Institute and State University, Blacksburg, VA, 1984

Beaton, R. and Farley, W., *Comparative Study of the MTFA, ICS and SQRI Image Quality Metrics for Visual Display Systems*, Armstrong Laboratory Report AL-TR-1992-0001, 1991.

Borough, H.C., Fallis, R.F., Warnock, R.H., and Britt, J.H. Quantitative determination of image quality. Boeing Company Report D2-114058-1, 1967.

Carlson, C.R. Sine-wave threshold contrast-sensitivity function: Dependence on display size. RCA Review, 43, 675-683, 1982.

Carlson, C.R. and Cohen, R.W. A simple psychophysical model for predicting the visibility of display information. Proceedings of the Society for Information Display, 21, 1980.

O'Callaghan, J.P. and Veron, H. Parametric MTF analysis for shadow-mask CRT monitor Configurations. Proceedings of the Society for Information Display, 28, 1987.

O'Callaghan, J.P. and Veron, H. A new approach for analyzing the visual-resolution characteristics of shadow-mask CRT monitor configurations. Proceedings of the Society for Information Display, 30, 1989.

Nyquist, H. Certain Factors Affecting Telegraph Speed. Bell System Technical Journal, April 1924.

Nyquist, H. Certain Topics in Telegraph Transmission Theory, A.I.E.E. Trans., V47, April 1928.

Park, S. K., Schowengerdt, R., and Kaczynski, M., Modulation-transfer-function analysis for sampled image systems, Applied Optics, V23 No. 15, August 1984.

Snyder, H.L. Image quality and observer performance, In L. M. Biberman (ed.), Perception of displayed information. New York; Plenum, 1973.

Snyder, H.L. Human visual performance and flat panel display image quality. Human Factors Laboratory Technical Report, HFL-80/ONR-80-1, Virginia Polytechnic Institute and State University, Blacksburg, VA, 1980.

Snyder, H.L. Image quality: Measures and visual performance. In, L.E. Tannas (ed.), Flat panel displays and CRTs, New York: Van Nostrand Reinhold, 1985.

van Meeteren, A. Visual aspects of image intensification. Ph.D. Dissertation, Univ. of Utrecht, The Netherlands, 1973.

Veron, H. and O'Callaghan, J.P. A technique for the automated measurement of the resolution of shadow-mask CRT displays. Proceedings of the Society for Information Display, 28, 1987.

Appendix A. Computer Model of Color CRT Models

The spatial imaging capacity of visual displays can be characterized by photometric measurements of target images presented on the screen. One popular type of target image is a one-pixel wide line. The luminance distribution across the width of this line image is known as the Line Spread Function (LSF). The LSF is used most often to determine in MTF of the display.

Another useful target image is a one-pixel on/one-pixel off (On-Off) grating pattern. For discretely addressed displays, the On-Off pattern represents the highest spatial frequency that the systems can transmit. Also, the On-Off pattern represents the highest spatial frequency point in the system's MTF. The On-Off pattern can be measured with the same photometric equipment as used for the line pattern.

The computer models developed for this work simulated the photometric measurements of line and On-Off patterns presented on phosphor dot and phosphor stripe color CRTs. The computer models allow several display device and measurement system parameters to be varied.

A.1 Phosphor Dot CRT Model

This section presents a mathematical system to simulated the luminance distributions associated with line and On-Off patterns on phosphor dot CRTs. The mathematical system was implemented as a computer program for the purposes of this work. The computer program is referred to as the Phosphor Dot CRT Model (PDCM), and it consists of four functions: PMLSF Function (PMLSFF), Location Function (LF), Dot Function (DF), and Aperture Function (AF).

A.1.a PMLSF Functions. The screen structure of a phosphor dot color CRT is shown in Figure A1. The spatial relationships of the PDM are referenced to an (x,y) Cartesian coordinate system, in which x refers to the horizontal dimension and y refers to the vertical dimension. The origin (0,0) is located at the center of a green-colored phosphor dot.

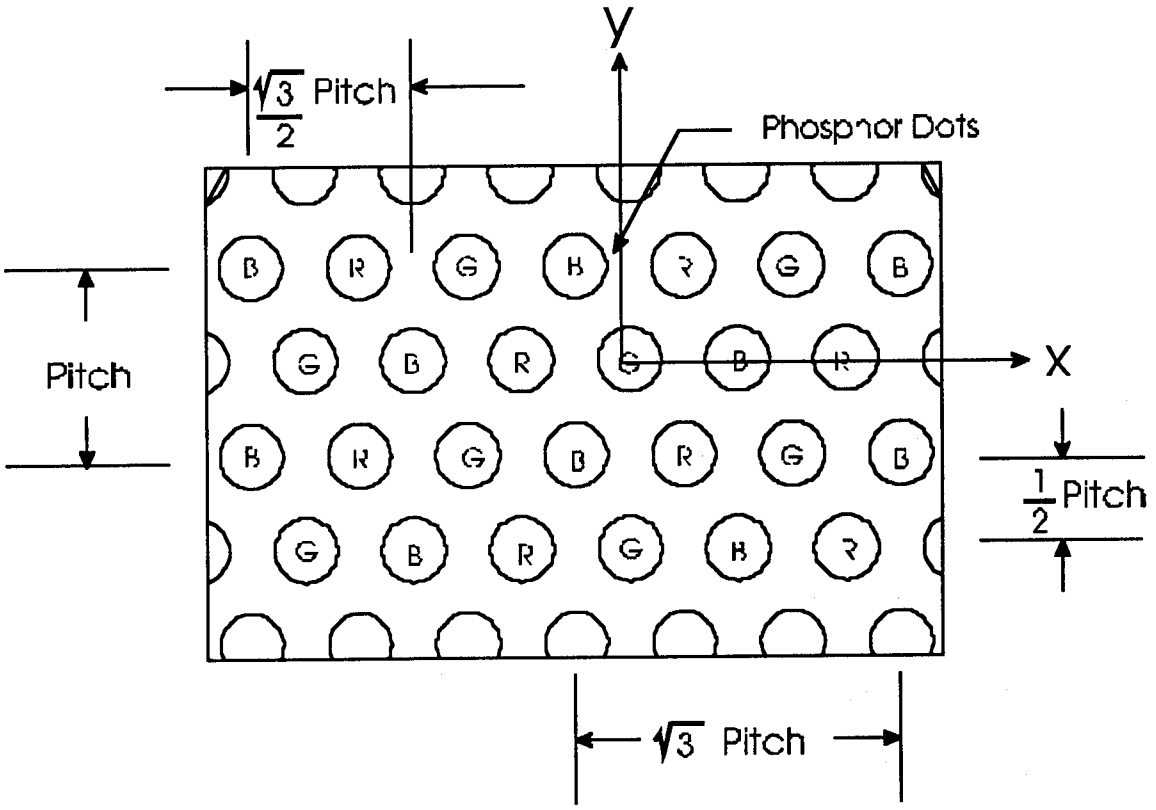

Figure A1. Screen structure of a phosphor dot color CRT.

As discussed elsewhere in the report, the PMLSF refers to the LSF before it is sampled by the phosphor dot pattern. The composite PMLSF of a color CRT consists of multiple PMLSF; one PMLSF for each electron gun. For typical color CRTs, there are three PMLSFs: red PMLSF, green PMLSF, and blue PMLSF. Thus,

$$PMLSF_c(x,y) = PMLSF_r + PMLSF_g + PMLSF_b \qquad \text{(Eq. A1)}$$

in which

$PMLSF_c$ denotes the composite PMLSF

$PMLSF_r$ denotes the red PMLSF,

$PMLSF_g$ denotes the green PMLSF, and

$PMLSF_b$ denotes the blue PMLSF

Because PMLSFs are Gaussian shaped in most color CRTs, we can write a set of analytical expressions to describe their two-dimension luminance profiles, as given below.

$$PMLSF_r(x,y) = I_r \exp\left[\frac{-4\ln 2(x+\Psi+\phi_r)^2}{w_r^2}\right] \quad \text{(Eq. A2)}$$

$$PMLSF_g(x,y) = I_g \exp\left[\frac{-4\ln 2(x+\Psi)^2}{w_g^2}\right] \quad \text{(Eq. A3)}$$

$$PMLSF_b(x,y) = I_b \exp\left[\frac{-4\ln 2(x+\Psi+\phi_b)^2}{w_b^2}\right] \quad \text{(Eq. A4)}$$

in which,

I_g denotes the intensity of the green electron beam,
I_r denotes the intensity of the red electron beam,
I_b denotes the intensity of the blue electron beam,
Ψ denotes the distance from the origin and the peak of green $PMLSF_g$,
ϕ_r denotes the distance from the peak of $PMLSF_g$ to the peak of $PMLSF_r$,
ϕ_b denotes the distance from the peak of $PMLSF_g$ to the peak of $PMLSF_b$,
w_g denotes the full width at half maximum intensity of the green line,
w_r denotes the full width at half maximum intensity of the red line, and
w_b denotes the full width at half maximum intensity of the blue line.

Eq. A2-A4 define the luminance distributions produced by red, green, and blue one-pixel wide lines displayed on a color CRT, without the influences of filtering by the phosphor dot structure. These equation also can be used to describe the luminance distributions across an On-Off grating pattern, as given below.

$$PMLP_r(x,y) = \sum_{n=j}^{k} I_r \exp\left[\frac{-4\ln 2(x+(ns_l)+\Psi+\phi_r)^2}{w_r^2}\right] \quad \text{(Eq. A5)}$$

$$PMLP_g(x,y) = \sum_{n=j}^{k} I_g \exp\left[\frac{-4\ln 2(x+(ns_l)+\Psi+\phi_g)^2}{w_g^2}\right] \quad \text{(Eq. A6)}$$

$$PMLP_b(x,y) = \sum_{n=j}^{k} I_b \exp\left[\frac{-4\ln 2(x+(ns_l)+\Psi+\phi_b)^2}{w_b^2}\right] \qquad \text{(Eq. A7)}$$

in which,

$PMLP_r$ denotes the red Pre-Mask Line Pattern,

$PMLP_g$ denotes the green Pre-Mask Line Pattern, and.

$PMLP_b$ denotes the blue Pre-Mask Line Pattern.

n denotes the line number,

j denotes the most negative line number to be considered,

k denotes the most positive line number to be considered, and

s_l denotes the line spacing.

A.1.b Dot Position Functions. Figure A1 shows that the phosphor dot CRT screen is composed of rows of repeating red, green, and blue dots. The horizontal spacing between same-colored phosphor dots is P_h. The even and odd rows are displaced horizontally from one another by $0.5P_h$. The center locations of the phosphor dots is this regular pattern are given by the set of equations below.

$$L_g(x,y) = \delta(x,y) \text{ if } \{ y = n P_V \text{ and } x = [\, m + \frac{1}{2} \text{mod2}(n) \,] P_h \} \qquad \text{(Eq. A8)}$$

$$L_r(x,y) = \delta(x,y) \text{ if } \{ y = n P_V \text{ and } x = [\, m + \frac{1}{3} + \frac{1}{2} \text{ mod2}(n) \,] P_h \} \qquad \text{(Eq. A9)}$$

$$L_r(x,y) = \delta(x,y) \text{ if } \{ y = n P_V \text{ and } x = [\, m + \frac{2}{3} + \frac{1}{2} \text{mod2}(n) \,] P_h \} \qquad \text{(Eq. A10)}$$

in which,

$L_g(x,y)$ denotes the green phosphor location function,

$L_r(x,y)$ denotes the red phosphor location function,

$L_b(x,y)$ denotes the blue phosphor location function,

n denotes the integer row number,

m denotes the integer location along the row,

P_V denotes the vertical or row pitch,

P_h denotes the horizontal dot pitch,

mod2() denotes the integer modulo function (i.e., 0 if even, 1 otherwise), and
$\delta(x,y)$ denotes the delta function (i.e., 1 if conditions are satisfied, 0 otherwise).

Eqs. A8-10 indicate the location of the center of a phosphor dot; that is, they equal 1 if the coordinate (x,y) is the center of a phosphor dot and equal 0 otherwise.

A.1.c Dot Region Functions. In the phosphor dot CRT, the dots themselves are assumed to be circular and uniform in shape. For simplification of the equations, it also is assumed that the luminance response properties are constant over the dot area. With these assumption, it is convenient to define the Dot Region Functions to indicate if an (x,y) coordinate is within the screen area occupied by a phosphor dot.

The Dot Functions may then be written as follows:

$$D_r(x,y) = \begin{vmatrix} 1 \text{ if } r_r^2 \le x^2 + y^2 \\ 0 \text{ otherwise} \end{vmatrix} \qquad \text{(Eq. A11)}$$

$$D_g(x,y) = \begin{vmatrix} 1 \text{ if } r_g^2 \le x^2 + y^2 \\ 0 \text{ otherwise} \end{vmatrix} \qquad \text{(Eq. A12)}$$

$$D_b(x,y) = \begin{vmatrix} 1 \text{ if } r_b^2 \le x^2 + y^2 \\ 0 \text{ otherwise} \end{vmatrix} \qquad \text{(Eq. A13)}$$

$$D(x,y) = \begin{vmatrix} 1 \text{ if } r^2 \le x^2 + y^2 \\ 0 \text{ otherwise} \end{vmatrix} \qquad \text{(Eq. A14)}$$

in which,

D_g, D_r, and D_b are defined to be the green, red, and blue Dot Region Functions,
D is the general Dot Region Function if all dots are the same size,

r_r is defined to be the radius of the red phosphor dots,
r_g is defined to be the radius of the green phosphor dots,
r_b is defined to be the radius of the blue phosphor dots, and
r is defined to be the radius of all dots if the dots are of equal size.

Equations A11-A14 assume that the origin is at the center of the phosphor dot.

A.1.d Aperture Function. The Aperture Function describes the spatial dimensions of a photometric measurement aperture. This equation may be written as follows:

$$A(x,y) = \begin{vmatrix} 1 \text{ if } a_w \le x \le 0 \text{ and } a_h \le y \le 0 \\ 0 \text{ otherwise} \end{vmatrix} \qquad \text{(Eq. A15)}$$

in which,
A denotes the Aperture Function,
L denotes the symbol for logical AND,
a_h denotes the aperture height, and
a_w denotes the aperture width.

As a_h and a_w decrease, the measurement approaches the actual LSF. Therefore, the fidelity of the LSF is controlled by setting a_h and a_w. For example, if the LSF is desired to an accuracy of 1.0 μm, a_h and a_w are set to 0.5 μm.

A.1.e Screen Sampling Functions. The Phosphor Dot Location Functions and Phosphor Dot Functions may be combined to give the Screen Sampling Functions. The Screen Sampling Function describes the two dimensional dot pattern on the CRT, as given below.

$$SS_g(x,y) = L_g(x,y) \otimes D_g(x,y) \qquad \text{(Eq. A16)}$$

$$SS_r(x,y) = L_r(x,y) \otimes D_r(x,y) \qquad \text{(Eq. A17)}$$

$$SS_b(x,y) = L_b(x,y) \otimes D_b(x,y) \qquad \text{(Eq. A18)}$$

in which,

SS_g, SS_r, and SS_b are the green, red, and blue SSFs, respectively and

□ is the convolution operator.

The convolution integral for Eqs. A16-A18 is written as follows:

$$SSF(x,y) = \int_{x_l}^{x_h} \int_{y_l}^{y_h} \partial(x-u)D(u,v)du\,d \qquad \text{(Eq. A19)}$$

in which,

x_l denotes the lower extent of the horizontal range,

x_h denotes the upper extent of the horizontal range,

y_l denotes the lower extent of the vertical range,

y_h denotes the upper extent of the vertical range, and

u and v denote the convolution variables.

The following equations describe the sampling of the Pre-Mask functions by the Screen Sampling Functions:

$$Line_g(x,y) = SS_g(x,y)\ PMLSF_g \qquad \text{(Eq. A20)}$$

$$Line_r(x,y) = SS_r(x,y)\ PMLSF_r \qquad \text{(Eq. A21)}$$

$$Line_b(x,y) = SS_b(x,y)\ PMLSF_b \qquad \text{(Eq. A22)}$$

$$LP_g(x,y) = SS_g(x,y)\ PMLP_g \qquad \text{(Eq. A23)}$$

$$LP_r(x,y) = SS_r(x,y)\ PMLP_r \qquad \text{(Eq. A24)}$$

$$LP_b(x,y) = SS_b(x,y)\ PMLP_b \qquad \text{(Eq. A25)}$$

in which,

LP_g, LP_r, and LP_b denote the green, red, and blue Line Patterns and

$Line_g$, $Line_r$, and $Line_b$ denote the two dimensional green, red, and blue lines.

The equations above describe the two dimensional phosphor dot structure of a color CRT display. The LSF, however, is considered as a one dimensional function in this work. Therefore, the LSF is computed by convolving the Line Functions ($Line_g$,$Line_r$, $Line_b$) with the Aperture Function in the x direction over the range of the PMLSF. This relationship is given below.

$$LSF_g(x) = Line_g(x,y) \otimes A(x,y) \text{ for all } x \qquad \text{(Eq. A26)}$$

$$LSF_r(x) = Line_r(x,y) \otimes A(x,y) \text{ for all } x \qquad \text{(Eq. A27)}$$

$$LSF_b(x) = Line_b(x,y) \otimes A(x,y) \text{ for all } x \qquad \text{(Eq. A28)}$$

A similar set of equations for the On-Off grating pattern is given below.

$$LP_g(x) = LP_g(x,y) \otimes A(x,y) \text{ for all } x \qquad \text{(Eq. A29)}$$

$$LP_r(x) = LP_r(x,y) \otimes A(x,y) \text{ for all } x \qquad \text{(Eq. A30)}$$

$$LP_b(x) = LP_b(x,y) \otimes A(x,y) \text{ for all } x \qquad \text{(Eq. A31)}$$

Eqs. A26-A31 define the luminance distributions of line and On-Off patterns as measured photometrically on a phosphor dot CRT. An ideal measurement of these patterns is approached as the size of the measurement aperture decreases. Using this fact, one may use Eqs. A26-A31 to model various effects due to the measurement system or display device parameters.

A.1.f Translation to Computer Algorithm. The equations described above provide a mathematical description of the imaging capacity of phosphor dot CRTs. Moreover, the equations provide a foundation computer algorithms to generate one- and two-dimensional LSFs and LPs. For this project, a computer program (C++) named DotLines() was developed to implement the PDOT model. The computer program used a discrete approximation to the continuous equations described above.

To describe the phosphor dot color CRT, DotLines() performs a discrete sampling operation over a specified (x,y) range of the CRT. The image-forming surface of the CRT is divided into a square grid. The center value of each square is used for all points within the square. Using this concept, two iteration loops, an x loop and a y loop, are employed to evaluate any rectangular area of the CRT.

To simplify the DotLines() program, the DOT_COLOR_CRT data structure and the DotScreenSampling() function were developed. The DOT_COLOR_CRT structure holds the phosphor dot parameters and functions.

The DotScreenSampling() function implements Eq. A19 in discrete form, as given below.

$$SS(x,y) = \sum_{x_l}^{x_h} \sum_{y_l}^{y_h} \partial(x-u, y-v) D(u,v) \Delta u \Delta v \qquad \text{(Eq. A32)}$$

Because $\delta(x,y)$ and $Dg(x,y)$ only have values of 0 and 1, the Screen Sampling Function only has values of 0 and 1; that is, Eq. A32 returns unity if the point is on a phosphor dot, otherwise it returns a zero value. Thus, the Sampling Function may be cast as a decision: either the (x,y) point is on a dot (1), or not on a dot (0).

DotLines() computes an LSF or LP by looping over a specified (x,y) range. The x value is taken as the scan length, whereas the y value is derived from the measurement aperture height. The number of steps in each direction is computed from the range and the step size. For each x-point, all y values are tested by DotScreenSampling() to determine if the y-point is on a phosphor dot. If any y-point is on a phosphor dot, the intensity is computed by the PMLSFF and accumulated. After the y-values have been computed for a given x-value, the accumulated luminance is placed in the x aperture array. The x aperture array is used to convolve the aperture width with the line pattern. This process is repeated for all x-values to yield the LSF or LP.

A.1.g Comparison Simulated and Actual LSF Measurements. To evaluate the fidelity of the phosphor dot CRT model, line and On-Off grating patterns computed by the model were compared with actual CRT measurements. For the actual

measurements, a phosphor dot CRT (Model: Viewsonic 7, P = 0.28 mm, 640 horizontal pixels) was measured with scanning microphotometer configured with a 3000.0 by 10.0 micron slit aperture. For the computed measurements, the model was programmed with same display and measurement system parameters as used in the actual measurements; although, the phase relationships in the model were determined empirically.

Figure A2 shows the results of the line test, which indicate that the model accurately computes the actual LSF measurement. The apparent differences between these LSFs stem from the facts that the model does not account for halation and glare background phenomena and it uses a perfect measurement aperture.

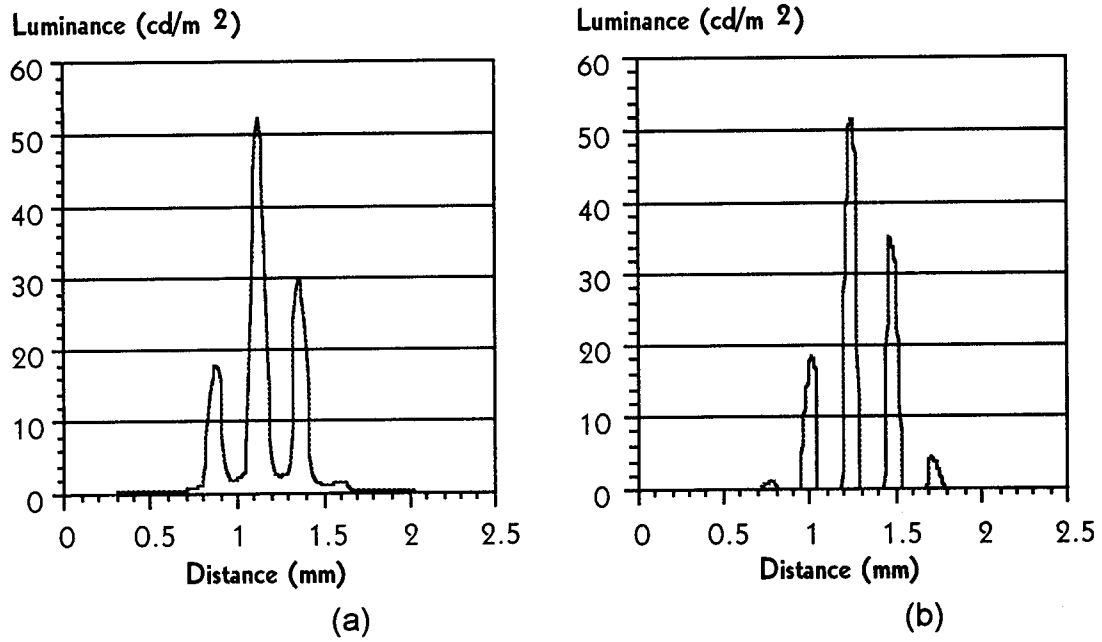

Figure A2. Comparison of measured and computed line patterns on a phosphor dot CRT. Part A shows the measured green line pattern for a Viewsonics 7 phosphor dot CRT. Part B shows the computed green line pattern using equivalent display device and measurement parameters.

Figure A3 shows the results of the On-Off grating pattern test. As shown, the model results fit the measured On-Off line pattern. The difference between the model and measured On-Off pattern stem from background luminance on the actual CRT.

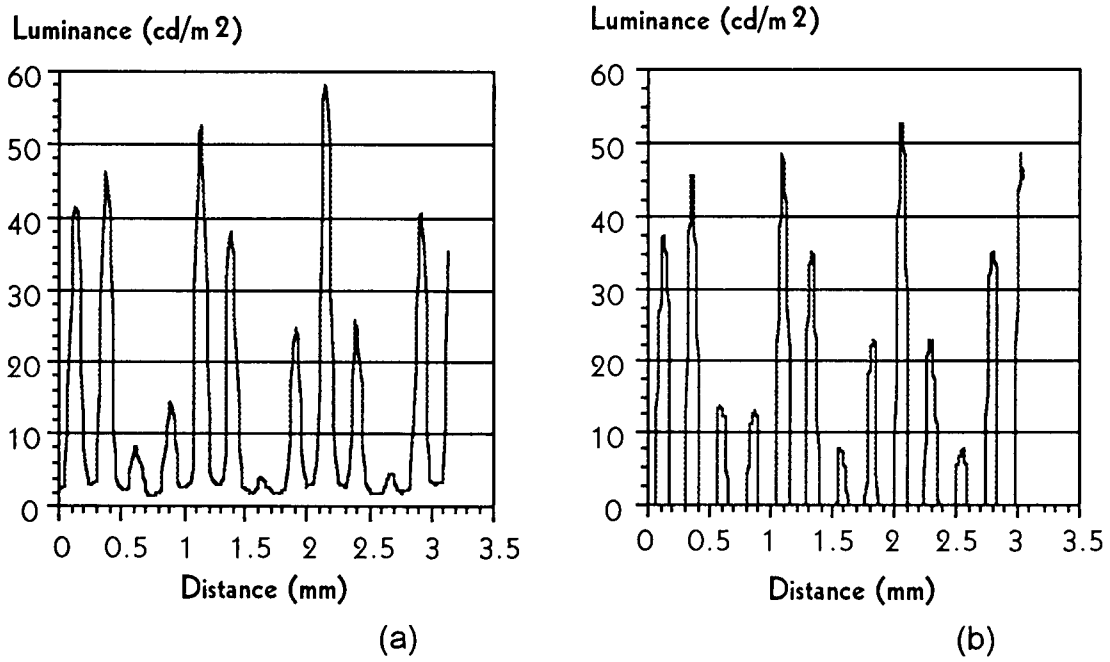

Figure A3. Comparison of measured and computed On-Off grating patterns on a phosphor dot CRT. Part A shows the measured green On-Off pattern for a Viewsonics 7 phosphor dot CRT. Part B shows the computed green On-Off pattern using equivalent display device and measurement parameters.

A.2 Phosphor Stripe CRT Model

The model of phosphor stripe CRTs is similar to that for phosphor dot CRTs, with the exception of the Dot Position and Region functions. The computer algorithm is referred to as the Phosphor Stripe CRT Model (PSCM).

A.2.a PMLSF Functions. Figure A4 illustrates the screen structure of phosphor stripe color CRTs. As shown, the phosphor stripe structure is continuous in the y-dimension and discrete in the x-dimension. Thus, PSCM was built as a one-dimensional model, rather than as a two-dimensional model used for PDCM. PSCM consists of four functions: PMLSF Function (PMLSFF), Stripe Location Function (SLF), Stripe Region Function (SRF), and the Aperture Function (AF). These functions reference a one-dimensional Cartesian coordinate system, which extends in a direction perpendicular to phosphor stripes. The origin of the coordinate system is located at the center of a green stripe.

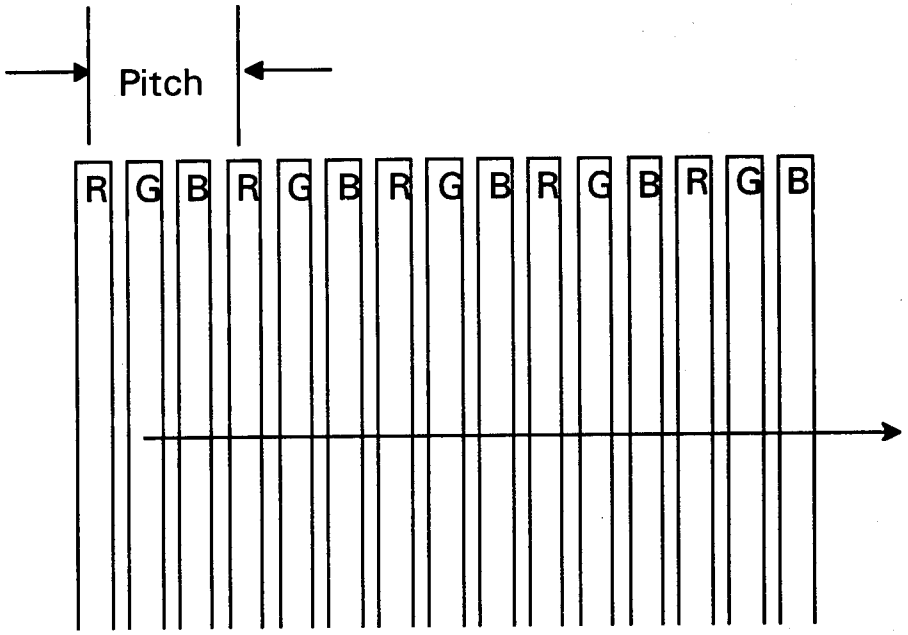

Figure A4. Screen structure of a phosphor stripe color CRT.

The PMLSFFs are identical for PSCM and PDCM, because the spot generated by the phosphor dot and stripe CRTs are identical prior to sampling by the phosphor structures.

A.2.b Stripe Position Functions. Because the PSCM is one dimensional, the stripe location functions are written as follows:

$$L_g(x) = \delta(x) \text{ if } \{ x = m\,P \} \qquad \text{(Eq. A33)}$$

$$L_r(x) = \delta(x) \text{ if } \{ x = [\, m + \tfrac{1}{3}]P \} \qquad \text{(Eq. A34)}$$

$$L_b(x) = \delta(x) \text{ if } \{ x = [\, m + \tfrac{2}{3}]\,P \} \qquad \text{(Eq. A35)}$$

in which,

$L_g(x)$ denotes the green phosphor location function,
$L_r(x)$ denotes the red phosphor location function,
$L_b(x)$ denotes the blue phosphor location function,
m denotes the integer stripe location,

P denotes the phosphor stripe pitch, and

$\delta(x)$ denotes the delta function (i.e., 1 if conditions are satisfied, 0 otherwise).

A.2.c Stripe Region Functions. The phosphor stripe functions are defined as follows:

$$S_r(x) = \left| \begin{array}{l} 1 \text{ if } s_r \le x \\ 0 \text{ otherwise} \end{array} \right| \qquad \text{(Eq. A36)}$$

$$S_g(x) = \left| \begin{array}{l} 1 \text{ if } s_g \le x \\ 0 \text{ otherwise} \end{array} \right| \qquad \text{(Eq. A37)}$$

$$S_b(x) = \left| \begin{array}{l} 1 \text{ if } s_b \le x \\ 0 \text{ otherwise} \end{array} \right| \qquad \text{(Eq. A38)}$$

$$S(x) = \left| \begin{array}{l} 1 \text{ if } s \le x^2 \\ 0 \text{ otherwise} \end{array} \right| \qquad \text{(Eq. A39)}$$

in which,

S_g, S_r, and S_b denote the green, red, and blue Stripe Functions,

S denotes the general Stripe Function if all stripes are the same size,

s_r denotes the width of the red phosphor stripes

s_g denotes the width of the green phosphor stripes

s_b denotes the width of the blue phosphor stripes

s denotes the width of all stripes if the stripes are of equal widths.

Eqs. A36-A39 assume that the origin is at the leading edge of the phosphor stripe.

A.2.d Aperture Function. The Aperture Function describes the measurement aperture used to obtain the LSF. This equation may be written as follows:

$$A(x) = \begin{vmatrix} 1 \text{ if } a_w \le x \le 0 \\ 0 \text{ otherwise} \end{vmatrix} \qquad \text{(Eq. A40)}$$

in which,

A denotes the aperture function and

a_W denotes the aperture width.

It is important to note that aperture height has no effect on the phosphor stripe CRT measurements since the stripes are uniform in the y-dimension. Thus, Eq. A40 is a one-dimensional function.

A.2.e Screen Sampling Functions. The Phosphor Stripe Location Function and Phosphor Stripe Functions may be combined to give the Phosphor Stripe Screen Sampling Functions. The Screen Sampling Functions describe the one dimensional stripe pattern of the phosphor stripe CRT.

$$SS_g(x) = L_g(x) \otimes S_g(x) \qquad \text{(Eq. A41)}$$

$$SS_r(x) = L_r(x) \otimes S_r(x) \qquad \text{(Eq. A42)}$$

$$SS_b(x) = L_b(x) \otimes S_b(x) \qquad \text{(Eq. A43)}$$

in which,

SS_g, SS_r, and SS_b denote the green, red, and blue SSFs, respectively.

The convolution integral for Eq. A41-A43 is written as follows:

$$SS(x) = \int_{x_l}^{x_h} \partial(x-u)S(u)\,du. \qquad \text{(Eq. A44)}$$

The following equations describe the sampling of the Pre-Mask functions by the Screen Sampling Functions:

$$Line_g(x) = SS_g(x)\ PMLSF_g \quad \text{(Eq. A45)}$$

$$Line_r(x) = SS_r(x)\ PMLSF_r \quad \text{(Eq. A46)}$$

$$Line_b(x) = SS_b(x)\ PMLSF_b \quad \text{(Eq. A47)}$$

$$LP_g(x) = SS_g(x)\ PMLP_g \quad \text{(Eq. A48)}$$

$$LP_r(x) = SS_r(x)\ PMLP_r \quad \text{(Eq. A49)}$$

$$LP_b(x) = SS_b(x)\ PMLP_b \quad \text{(Eq. A50)}$$

The final set of equations include the measurement aperture. The following equations describe the LSFs and LPs for the phosphor stripe CRT:

$$LSF_g(x) = Line_g(x) \otimes A(x) \text{ for all } x \quad \text{(Eq. A51)}$$

$$LSF_r(x) = Line_r(x) \otimes A(x) \text{ for all } x \quad \text{(Eq. A52)}$$

$$LSF_b(x) = Line_b(x) \otimes A(x) \text{ for all } x \quad \text{(Eq. A53)}$$

$$LP_g(x) = LP_g(x) \otimes A(x) \text{ for all } x \quad \text{(Eq. A54)}$$

$$LP_r(x) = LP_r(x) \otimes A(x) \text{ for all } x \quad \text{(Eq. A55)}$$

$$LP_b(x) = LP_b(x) \otimes A(x) \text{ for all } x \quad \text{(Eq. A56)}$$

As the aperture is made smaller, the ideal measurement system is approached. This allows the luminance pattern of the phosphor stripe CRT to be modeled to any desired accuracy.

A.2.f Translation to Computer Algorithm. The phosphor stripe equations were translated into a computer algorithm. This translation was similar to that used for the DotLines() function; however, the phosphor stripe program is called StripeLines().

A.2.f Translation to Computer Algorithm. The phosphor stripe equations were translated into a computer algorithm. This translation was similar to that used for the DotLines() function; however, the phosphor stripe program is called StripeLines().

The StripeLines() function implements Eq. 44 in discrete form, as given by

$$SS(x) = \sum_{x_l}^{x_h} \partial(x - u)S(u)\Delta u \qquad \text{(Eq. A57)}$$

StripeScreenSampling() returns a 0 if the x point is not on a stripe and a 1 if the x point is on the stripe.

Also, StripeLines() uses the StripeScreenSampling() and the PMLSF or PMLF to compute the LSF and LF. This computation is accomplished by looping over the range of x values at a specified step size. For each value of x, the StripeScreenSampling() is used to determine if the point is on a stripe. If it is on a stripe, the PMLSF or PMLF is used to compute the luminance of the point. If the point is not on a stripe, the luminance value is set to zero. After the luminance is computed, the value is placed in the aperture array. The aperture array is used to convolve the aperture width with the LSF or LF.

A.2.g Comparison Simulated and Actual LSF Measurements. To evaluate the fidelity of the phosphor stripe CRT model, a line pattern computed by the model were compared with actual CRT measurements. For the actual measurements, a phosphor stripe CRT (Model: Sony Trinitron□ Model GDM1950, P = 0.31 mm, 483 mm diagonal) was measured with scanning microphotometer configured with a 3000.0 by 10.0 micron slit aperture. For the computed measurements, the model was programmed with same display and measurement system parameters as used in the actual measurements; although, the phase relationships in the model were determined empirically.

Figure A5 shows the results of the line test, which indicate that the model accurately computes the actual LSF measurement. The apparent differences between these LSFs stem from the facts that the model does not account for halation and glare background phenomena and it uses a perfect measurement aperture.

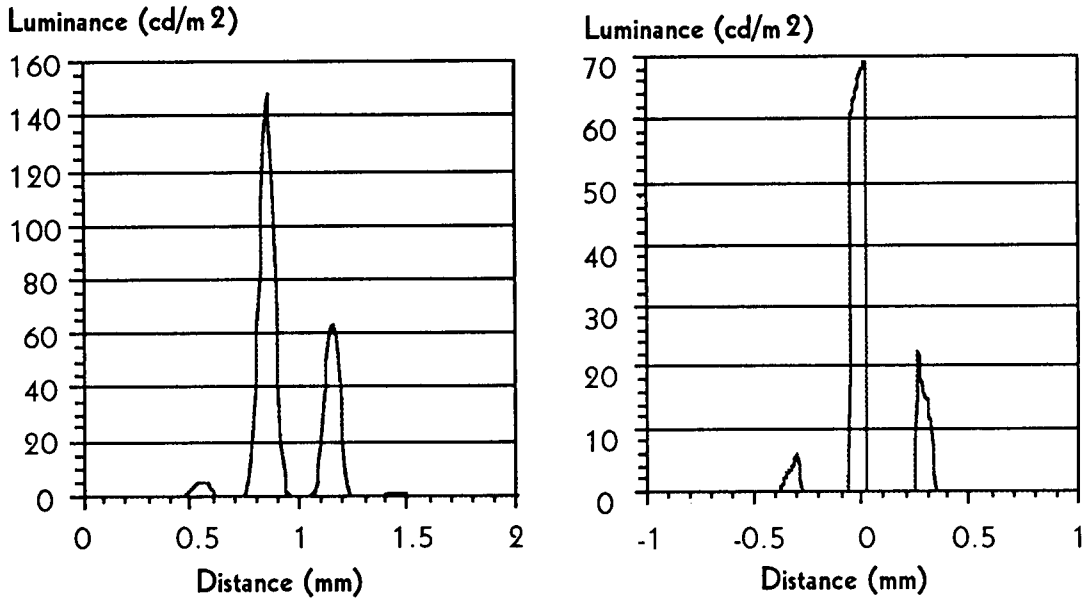

Figure A5. Comparison of measured and computed line patterns on a phosphor stripe CRT. Part A shows the measured green line pattern for a Sony phosphor dot CRT. Part B shows the computed green line pattern using equivalent display device and measurement parameters.

Appendix B. Effect of Color CRT Misconvergence on MTF

This appendix presents a set of stimulated LSFs and their associated MTFs for color CRTs with varying degrees of red and blue misconvergence.

The color CRT parameters used in the simulation analysis are listed Table B1. The various levels of red and blue misconvergence were combined factorially to define 25 analysis conditions. For each condition, the LSF and its MTF were computed. The MTFA, SQRI, and ICS values for each of the conditions are presented in the report.

Table B1. Color CRT Display Parameters used in Misconvergence Analysis

Display Parameter	**Description**
Screen diagonal	381 mm (15 inch)
Addressability	1024 horizontal pixels
RAR	1.0
FWHM	0.297 mm
Red misconvergence	-0.297, -0.149, 0.0, 0.149, and 0.297 mm
Blue misconvergence	-0.297, -0.149, 0.0, 0.149, and 0.297 mm
Viewing distance	550 mm (21.7 inches)

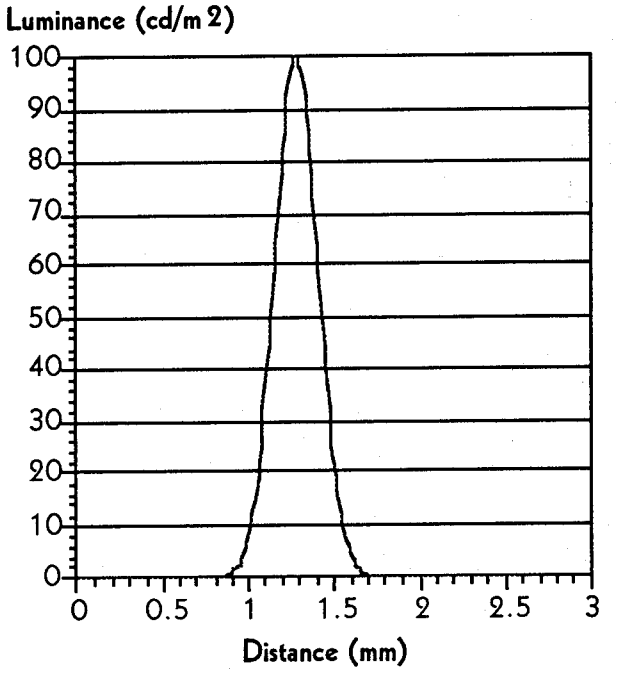

(a)

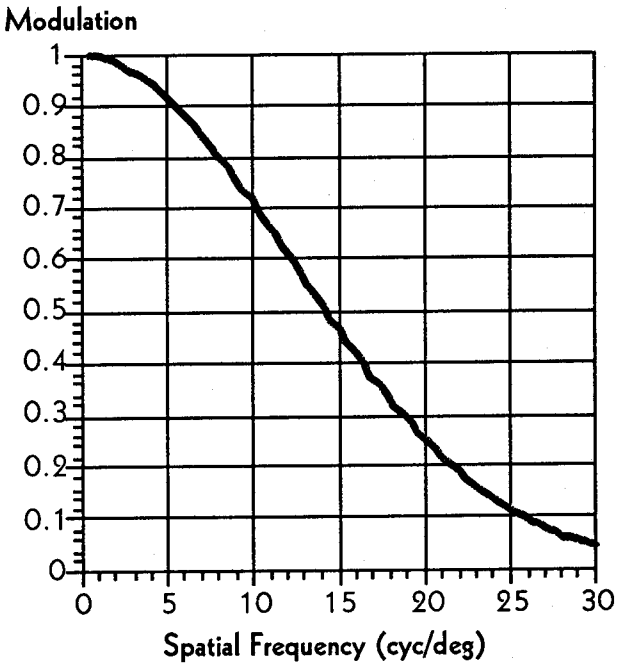

(b)

Figure B-1. Baseline LSF (a) and associated MTF (b) with no red and blue misconvergence.

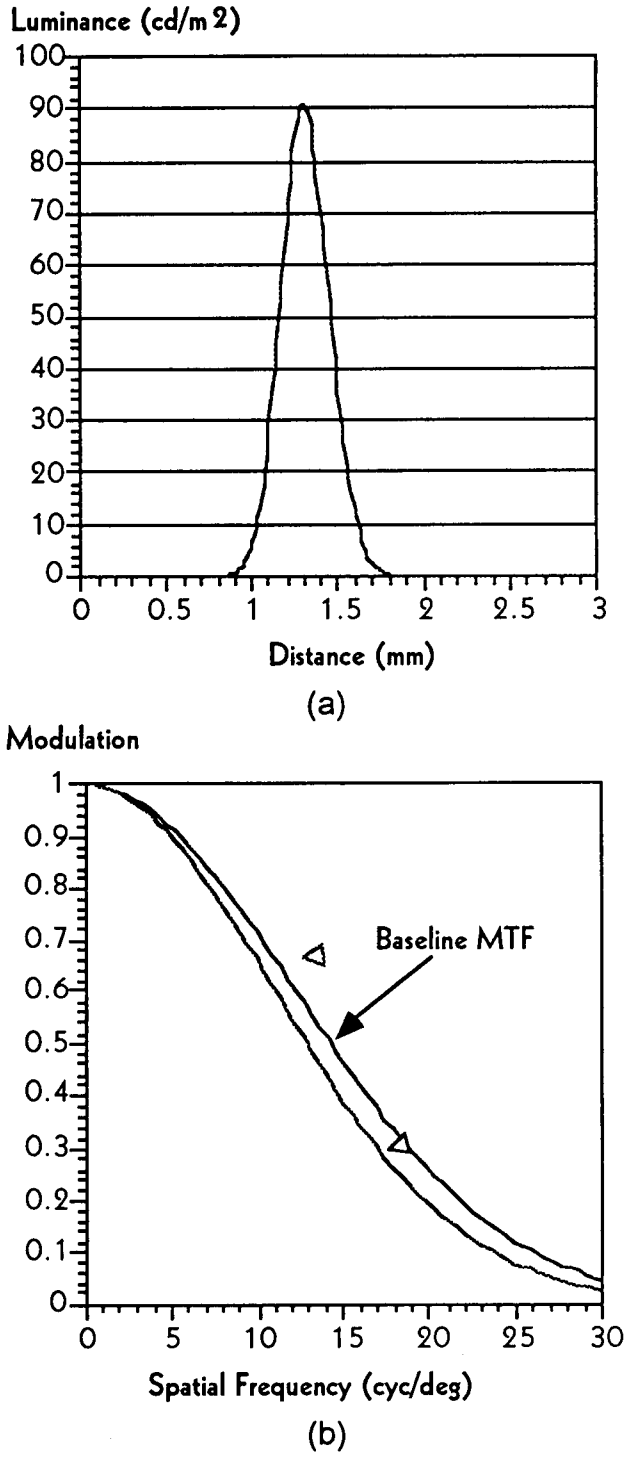

Figure B-2. Computed LSF (a) and associated MTF (b) for red misconvergence of -0.1488 mm and blue Misconvergence of 0 mm.

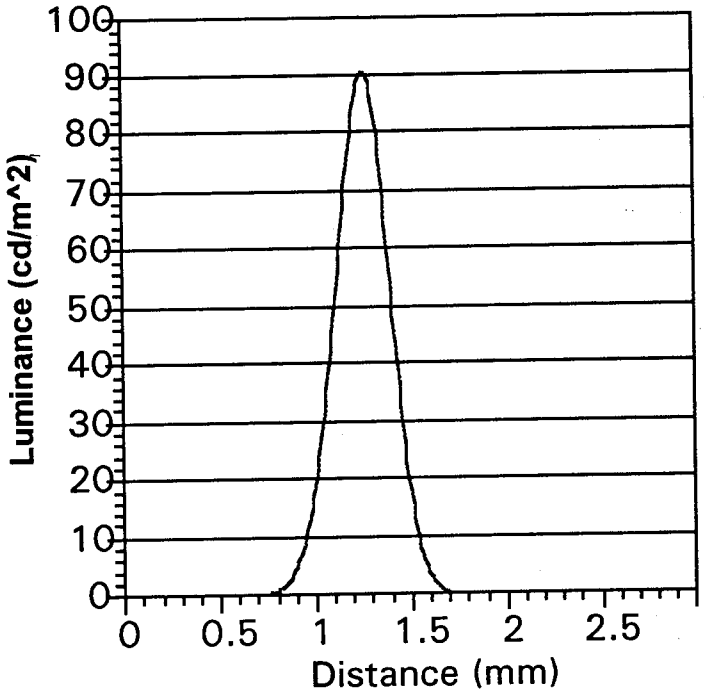

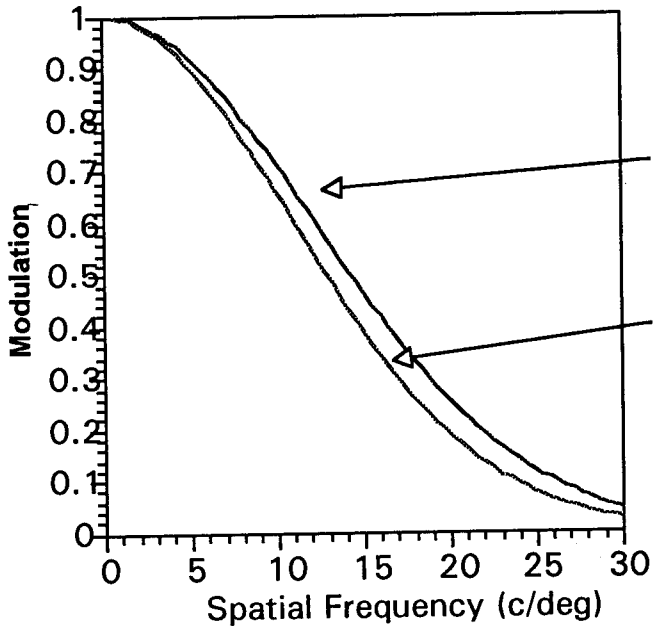

Figure B-3. LSF and Resulting MTF with 0.1488 mm of Red Misconvergence and No Blue Misconvergence Compared to the Converged MTF of Figure B1

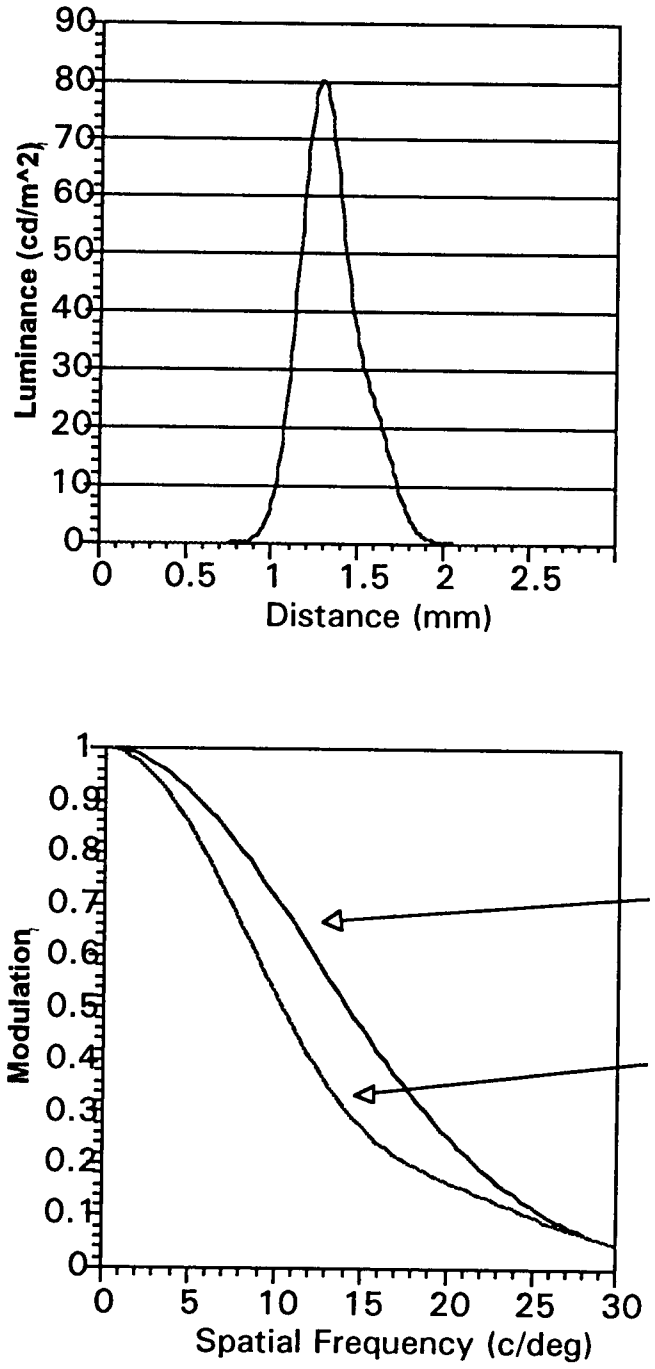

Figure B-4. LSF and Resulting MTF with -0.29765 mm of Red Misconvergence and No Blue Misconvergence Compared to the Converged MTF of Figure B1

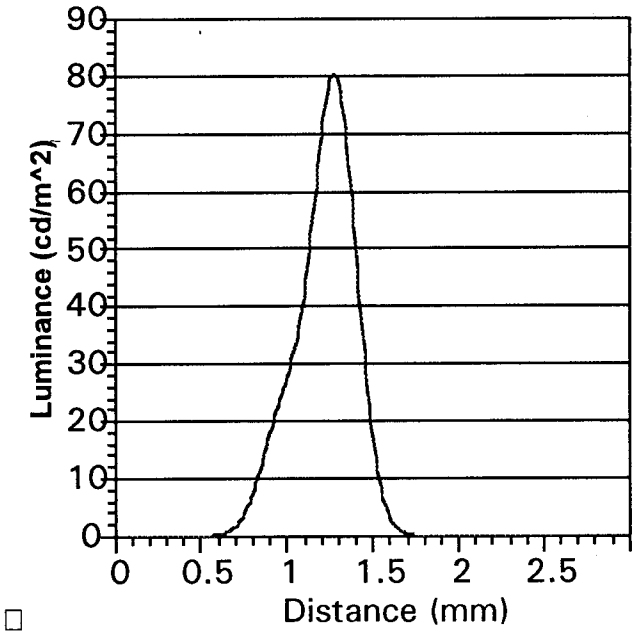

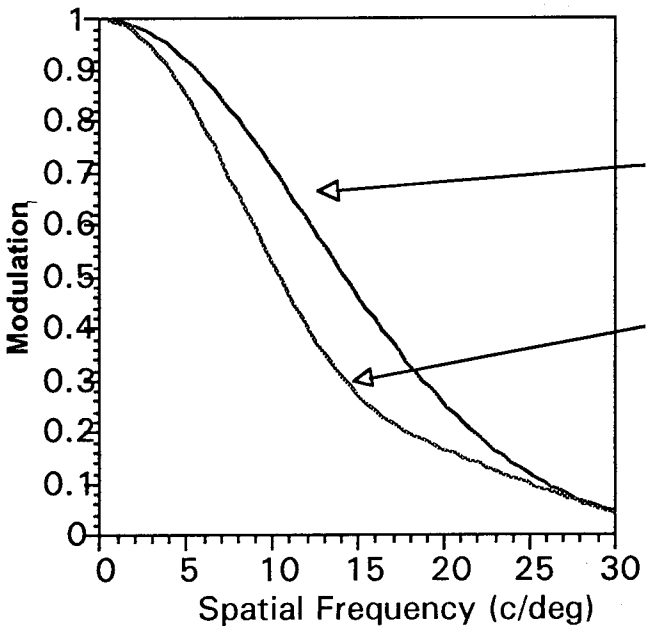

Figure B-5. LSF and Resulting MTF with 0.29765 mm of Red Misconvergence and No Blue Misconvergence Compared to the Converged MTF of Figure B1

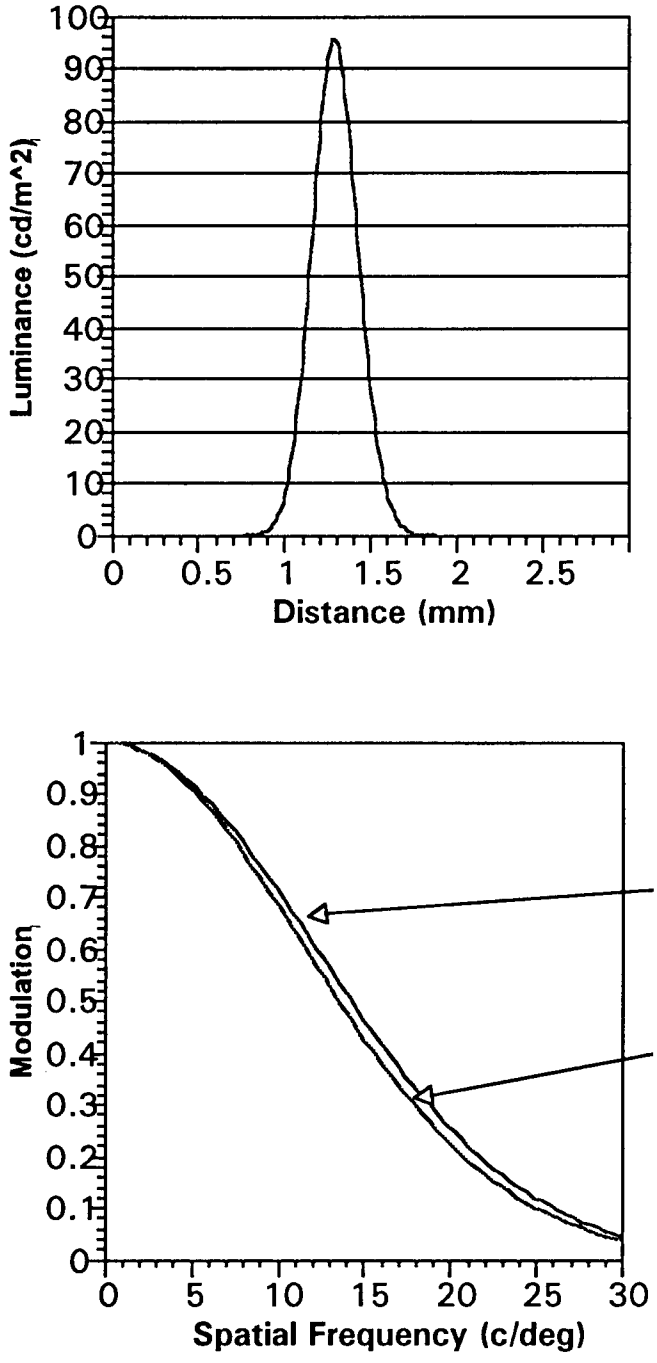

Figure B-6. LSF and Resulting MTF with 0.0 mm of Red Misconvergence and -0.1488 of Blue Misconvergence Compared to the Converged MTF of Figure B1

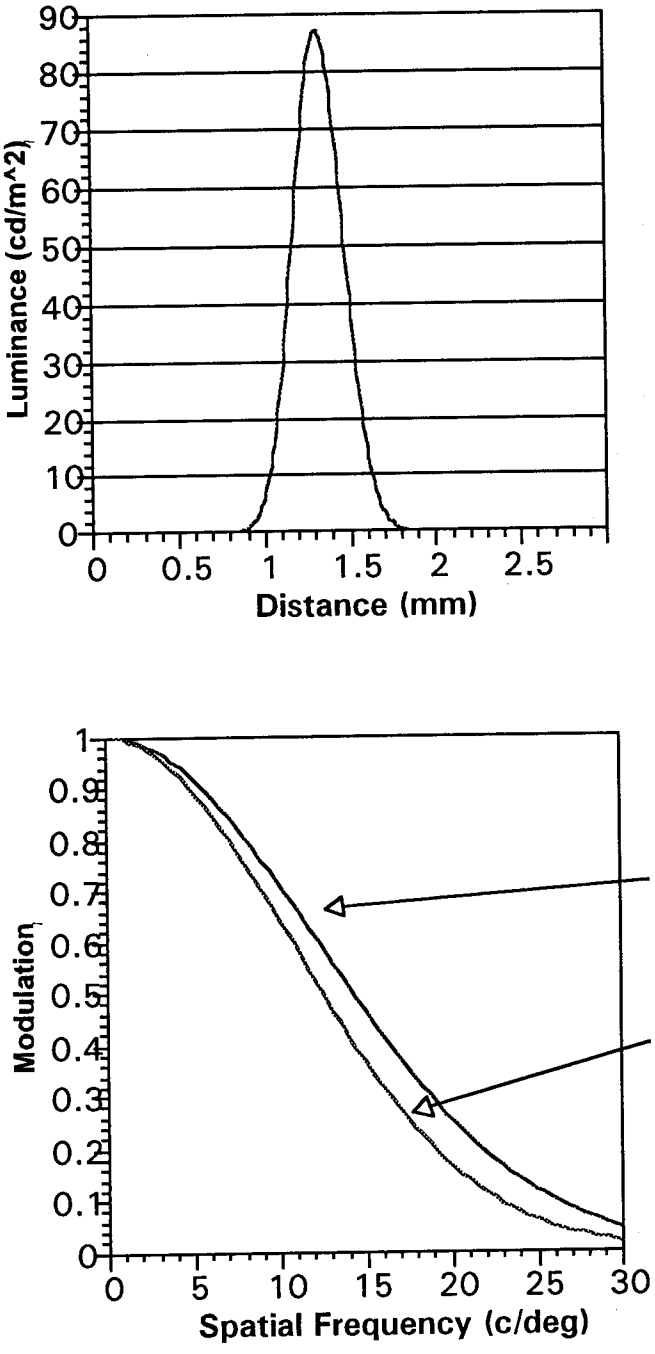

Figure B-7. LSF and Resulting MTF with -0.1488 mm of Red Misconvergence and -0.1488 of Blue Misconvergence Compared to the Converged MTF of Figure B1

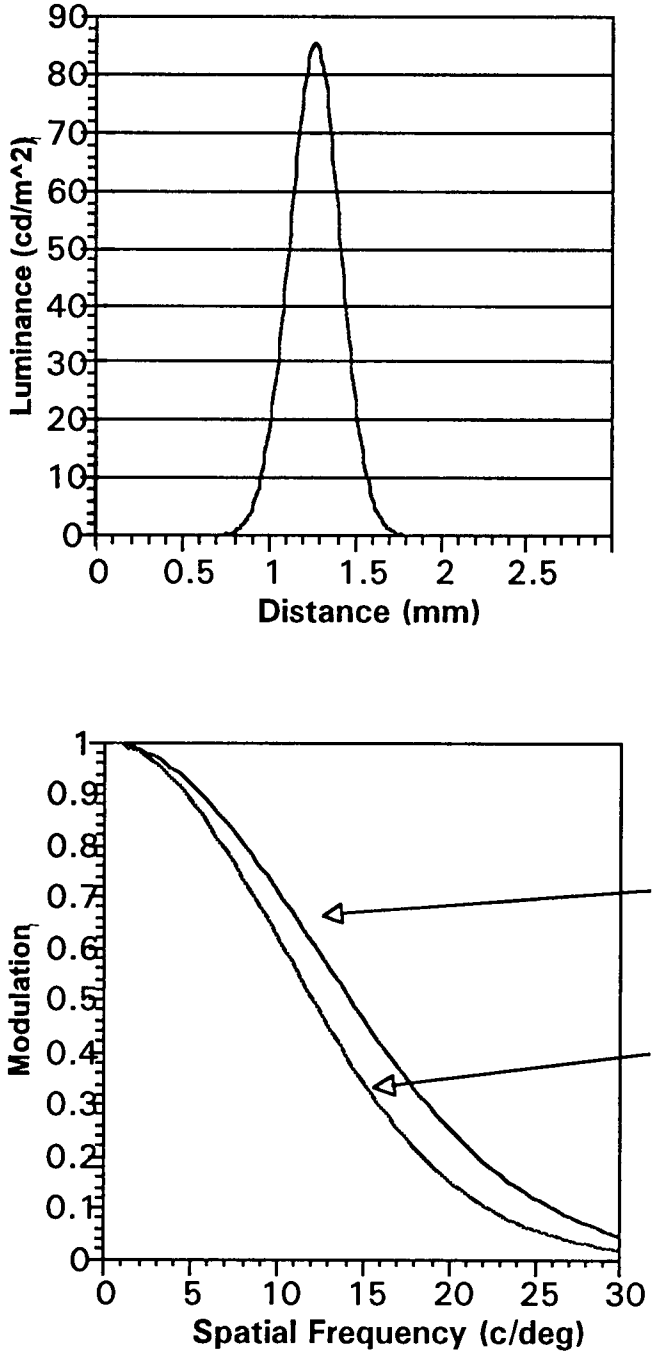

Figure B-8. LSF and Resulting MTF with 0.1488 mm of Red Misconvergence and -0.1488 of Blue Misconvergence Compared to the Converged MTF of Figure B1

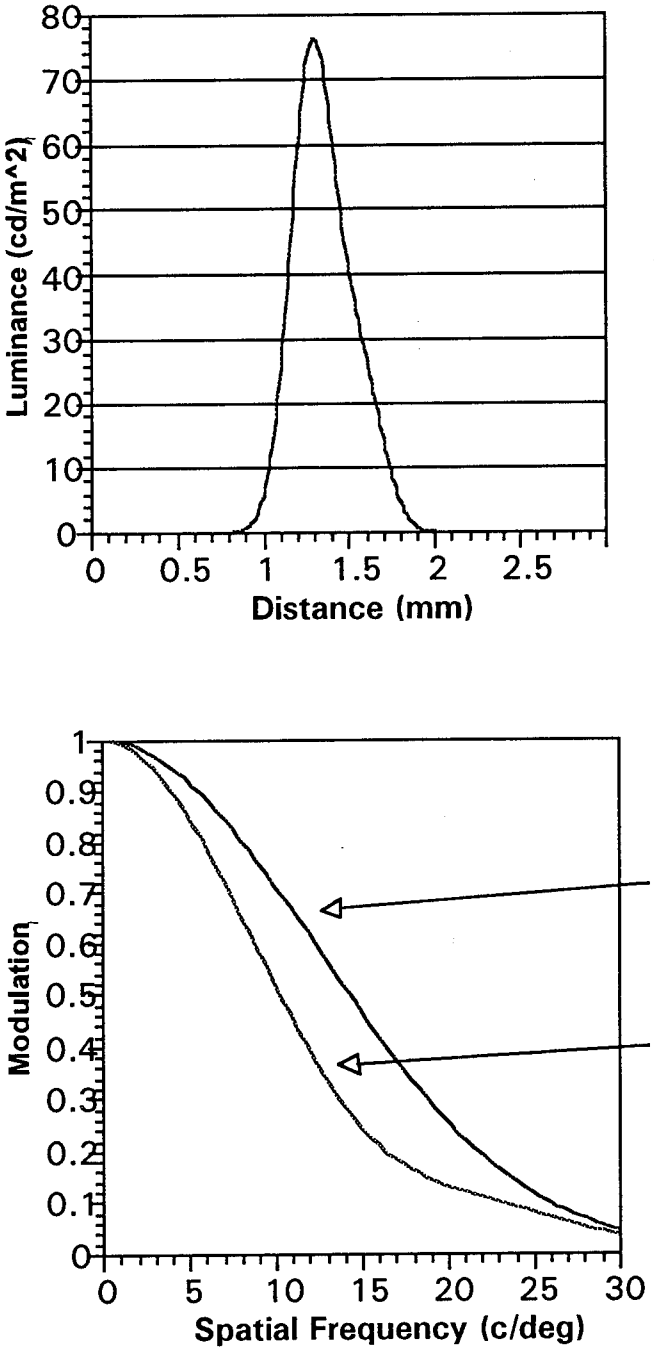

Figure B-9. LSF and Resulting MTF with -0.29765 mm of Red Misconvergence and -0.1488 of Blue Misconvergence Compared to the Converged MTF of Figure B1

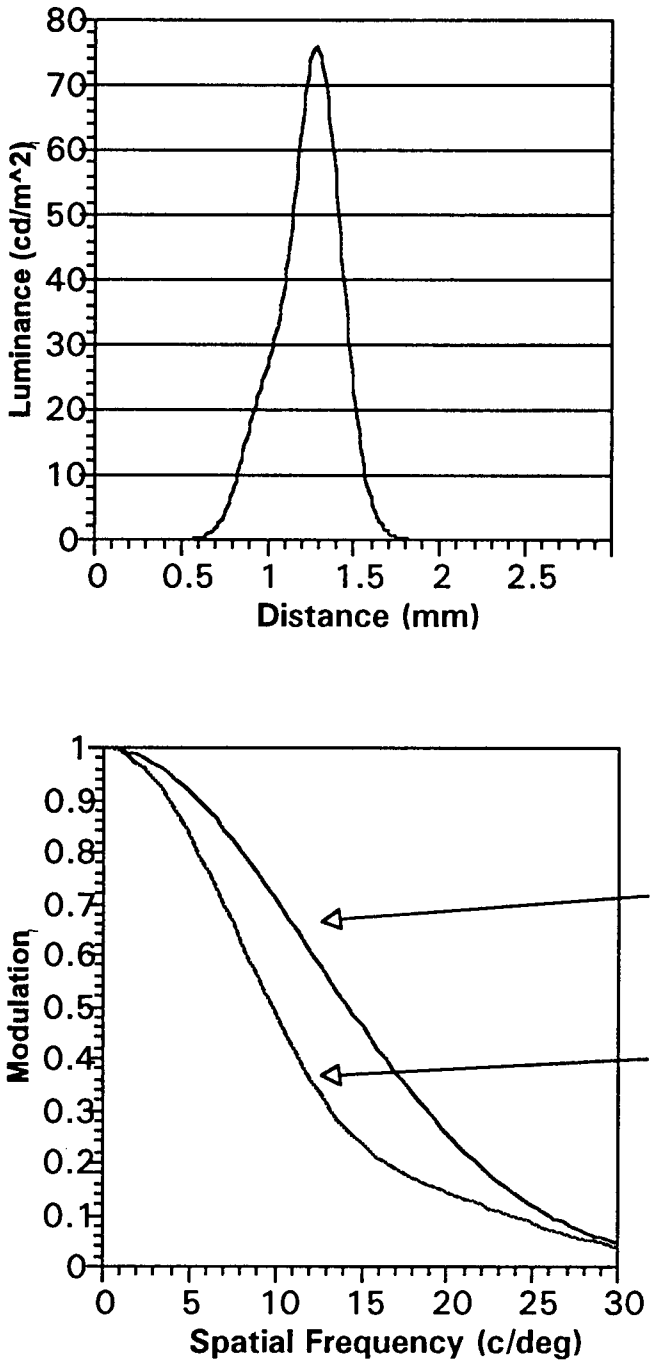

Figure B-10. LSF and Resulting MTF with 0.29765 mm of Red Misconvergence and -0.1488 of Blue Misconvergence Compared to the Converged MTF of Figure B1.

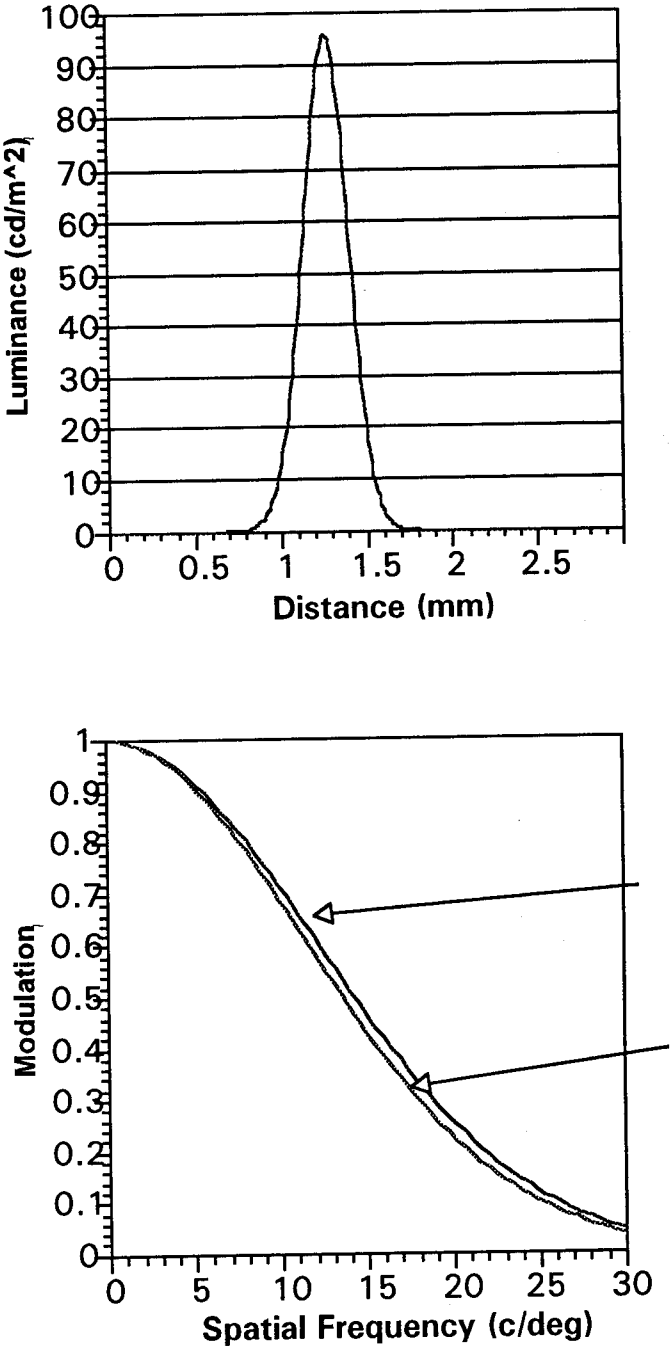

Figure B-11. LSF and Resulting MTF with 0.0 mm of Red Misconvergence and 0.1488 of Blue Misconvergence Compared to the Converged MTF of Figure B1.

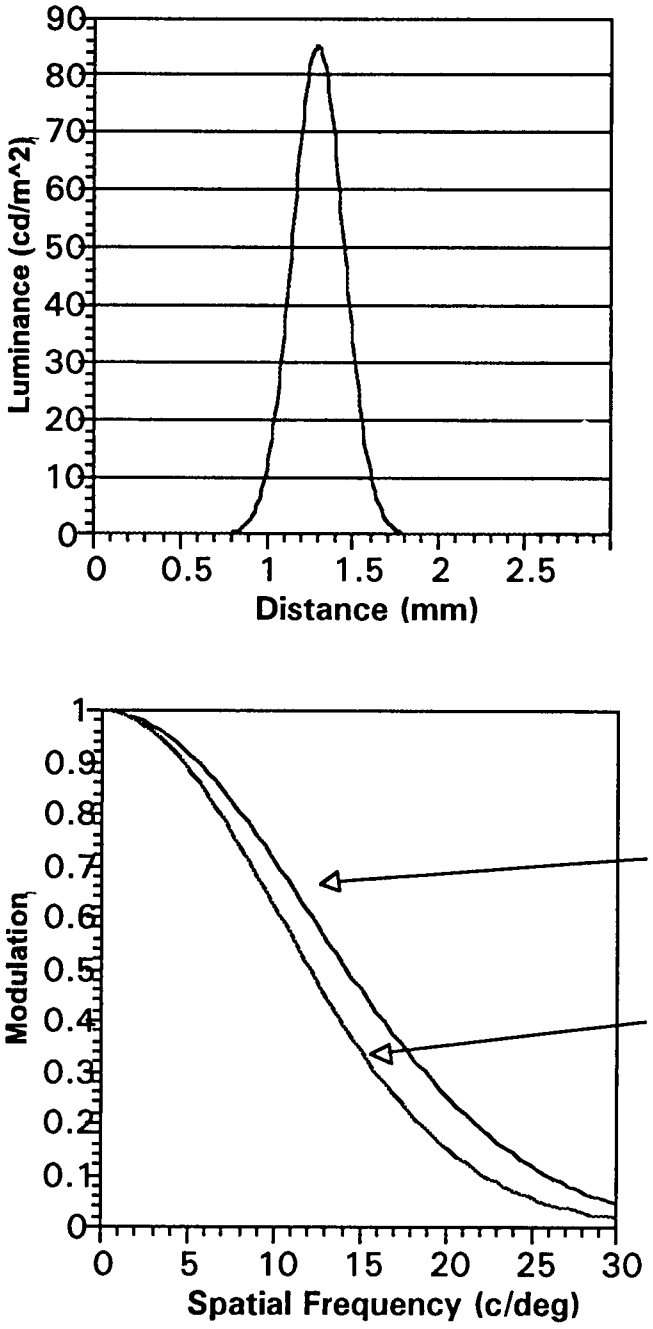

Figure B-12. LSF and Resulting MTF with -0.1488 mm of Red Misconvergence and 0.1488 of Blue Misconvergence Compared to the Converged MTF of Figure B1.

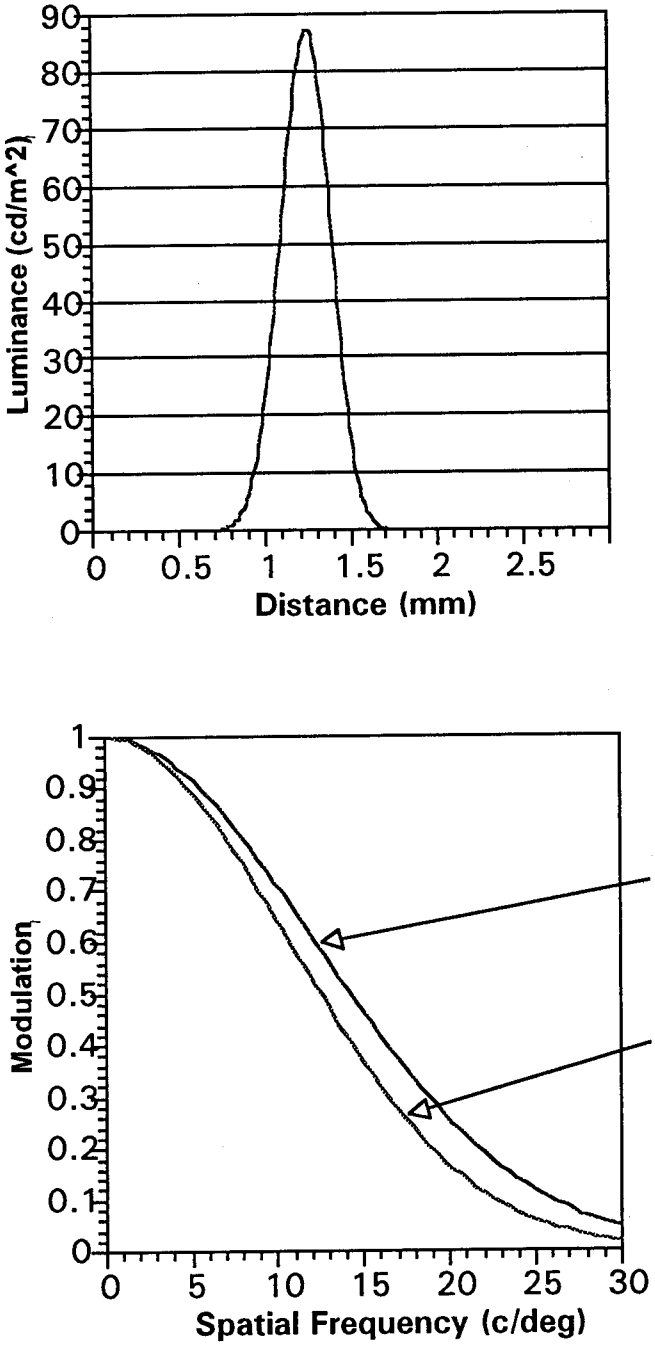

Figure B-13. LSF and Resulting MTF with 0.1488 mm of Red Misconvergence and 0.1488 of Blue Misconvergence Compared to the Converged MTF of Figure B1.

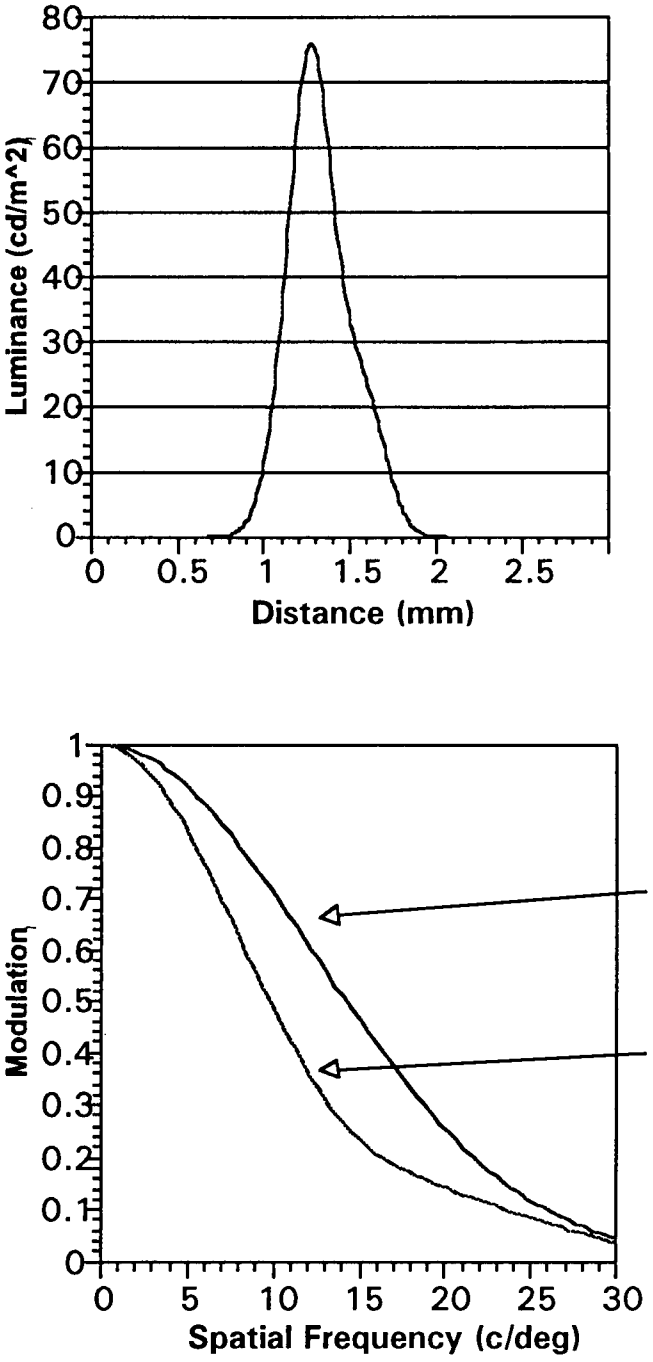

Figure B-14. LSF and Resulting MTF with -0.29765 mm of Red Misconvergence and 0.1488 of Blue Misconvergence Compared to the Converged MTF of Figure B1.

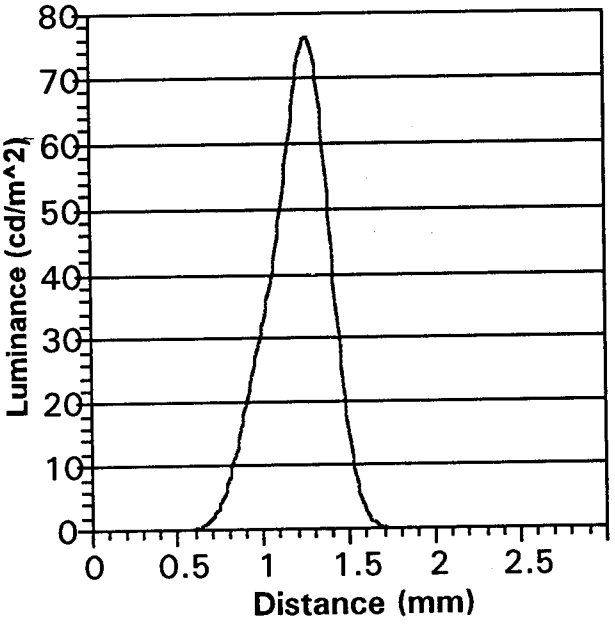

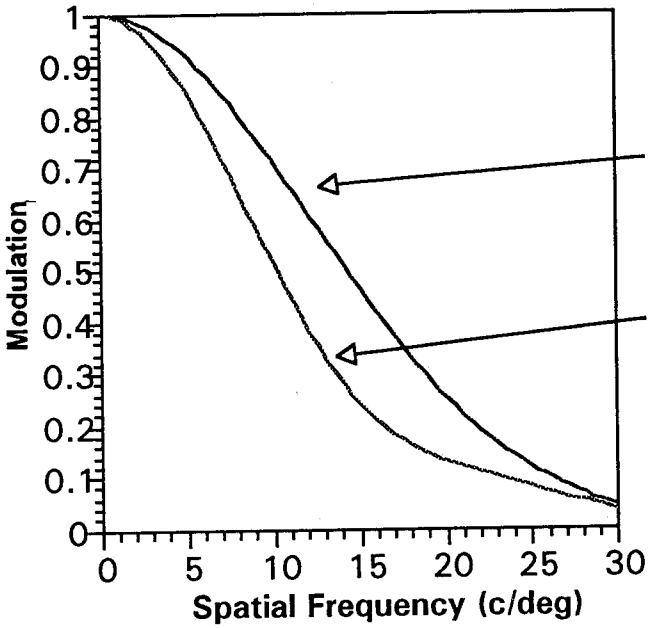

Figure B-15. LSF and Resulting MTF with 0.29765 mm of Red Misconvergence and 0.1488 of Blue Misconvergence Compared to the Converged MTF of Figure B1.

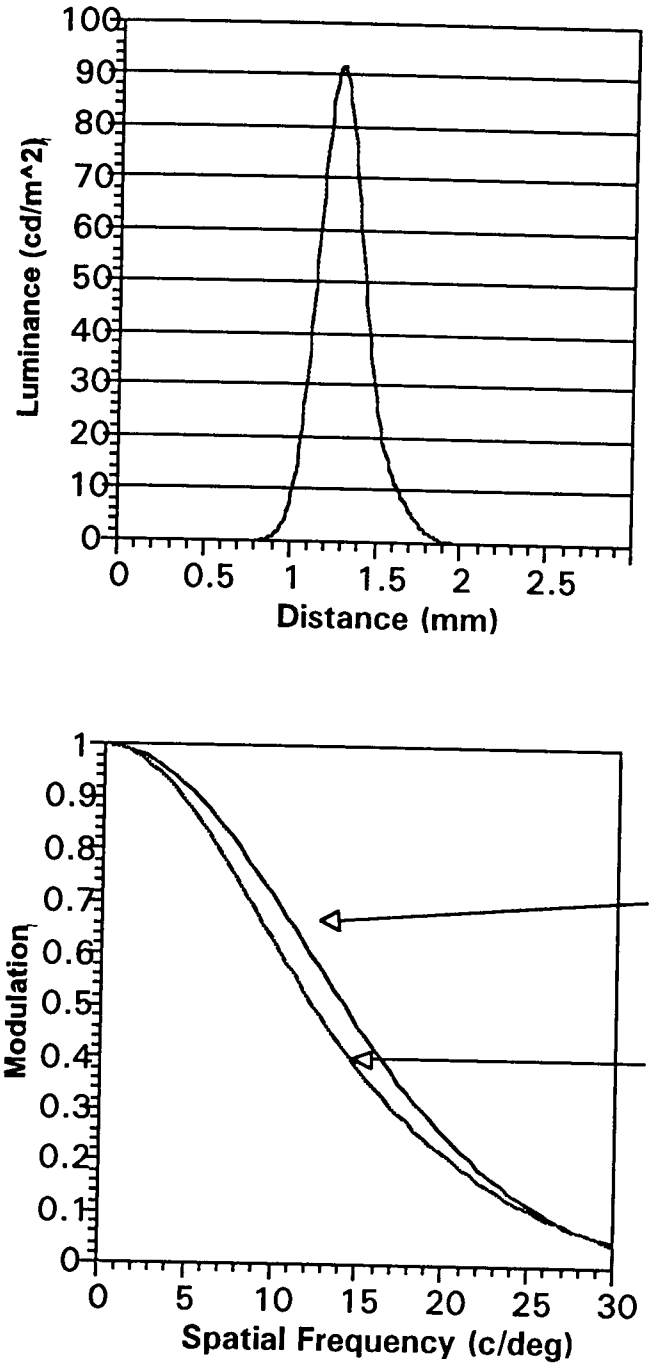

Figure B-16. LSF and Resulting MTF with 0.0 mm of Red Misconvergence and -0.29765 of Blue Misconvergence Compared to the Converged MTF of Figure B1.

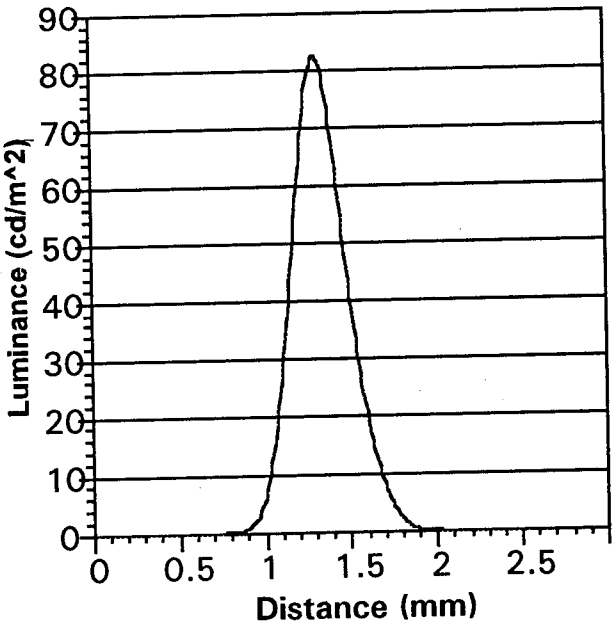

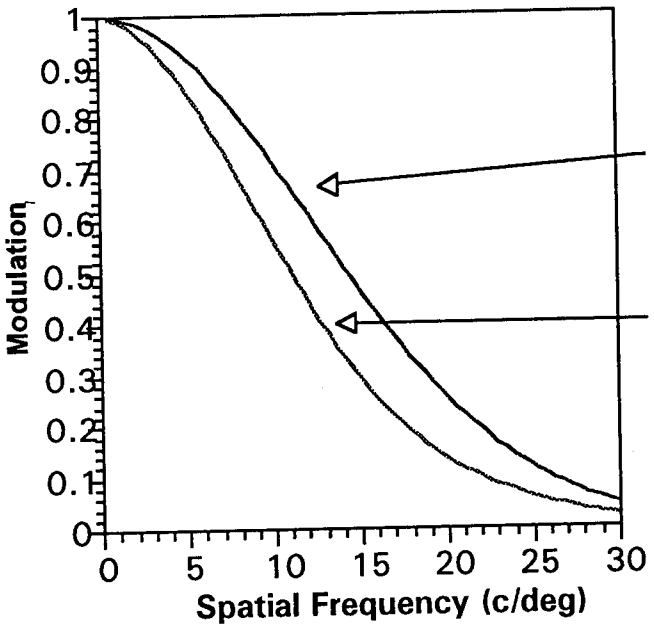

Figure B-17. LSF and Resulting MTF with -0.1488 mm of Red Misconvergence and -0.29765 of Blue Misconvergence Compared to the Converged MTF of Figure B1.

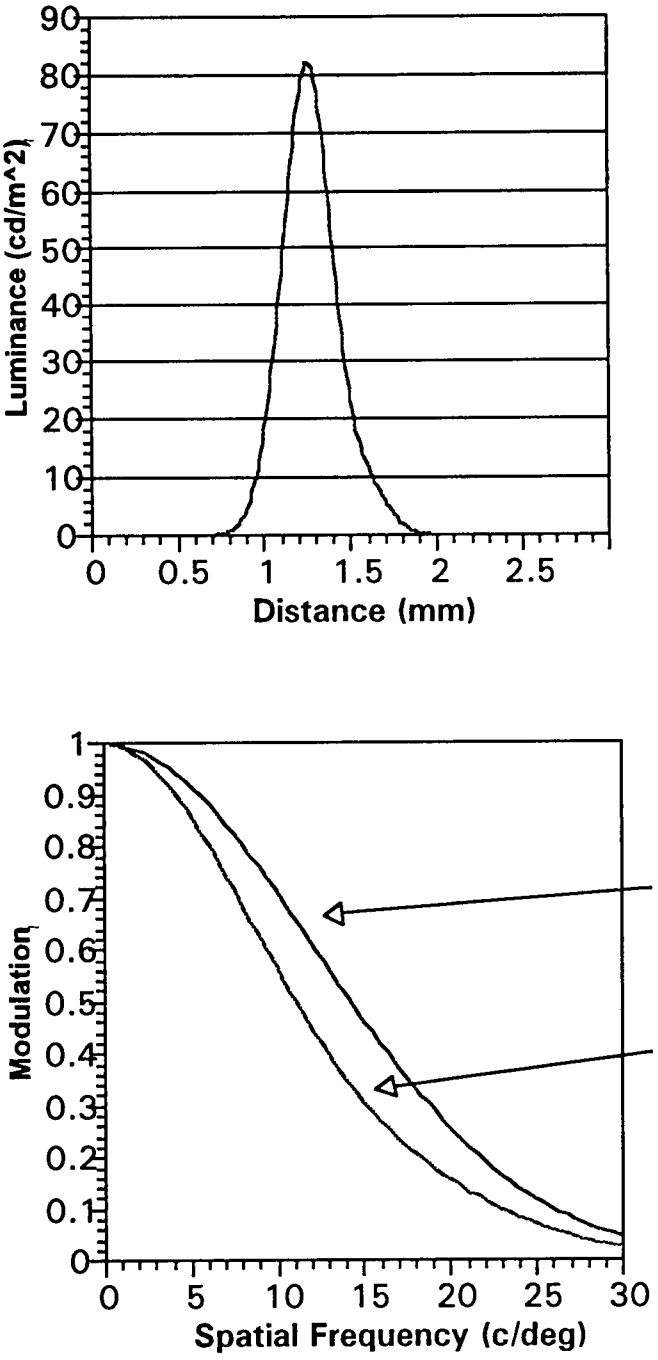

Figure B-18. LSF and Resulting MTF with 0.1488 mm of Red Misconvergence and -0.29765 of Blue Misconvergence Compared to the Converged MTF of Figure B1.

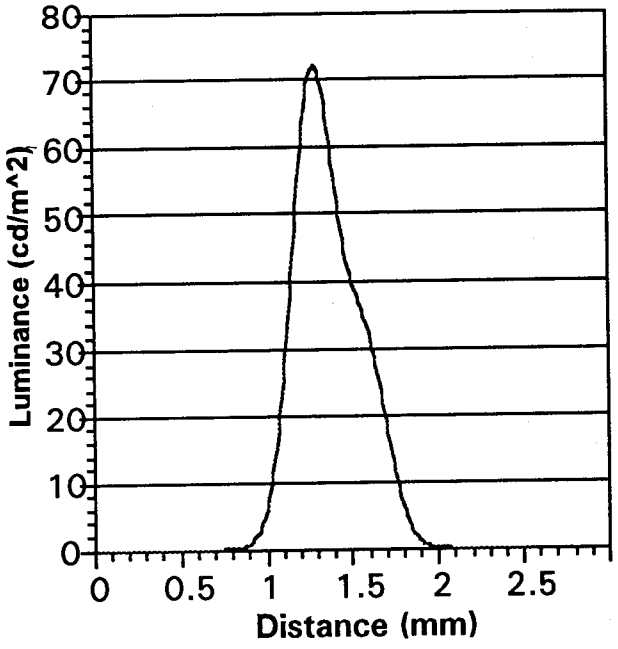

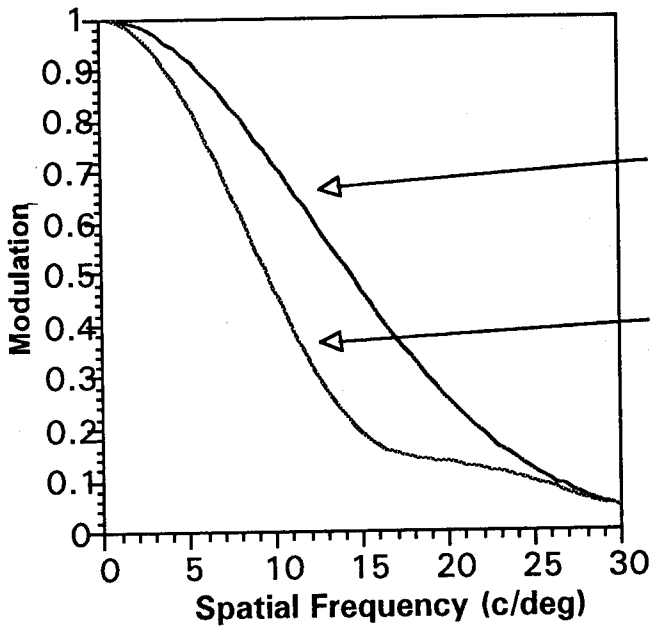

Figure B-19. LSF and Resulting MTF with -0.29765 mm of Red Misconvergence and -0.29765 of Blue Misconvergence Compared to the Converged MTF of Figure B1.

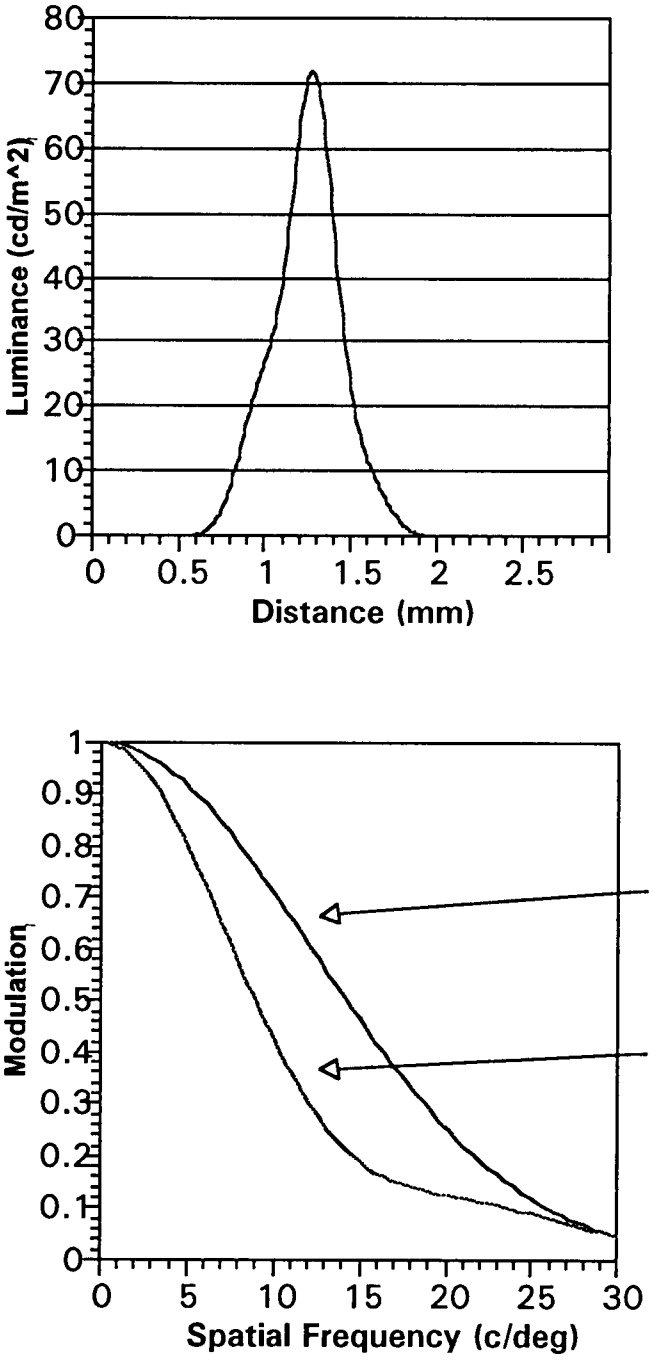

Figure B-20. LSF and Resulting MTF with -0.29765 mm of Red Misconvergence and -0.29765 of Blue Misconvergence Compared to the Converged MTF of Figure B1.

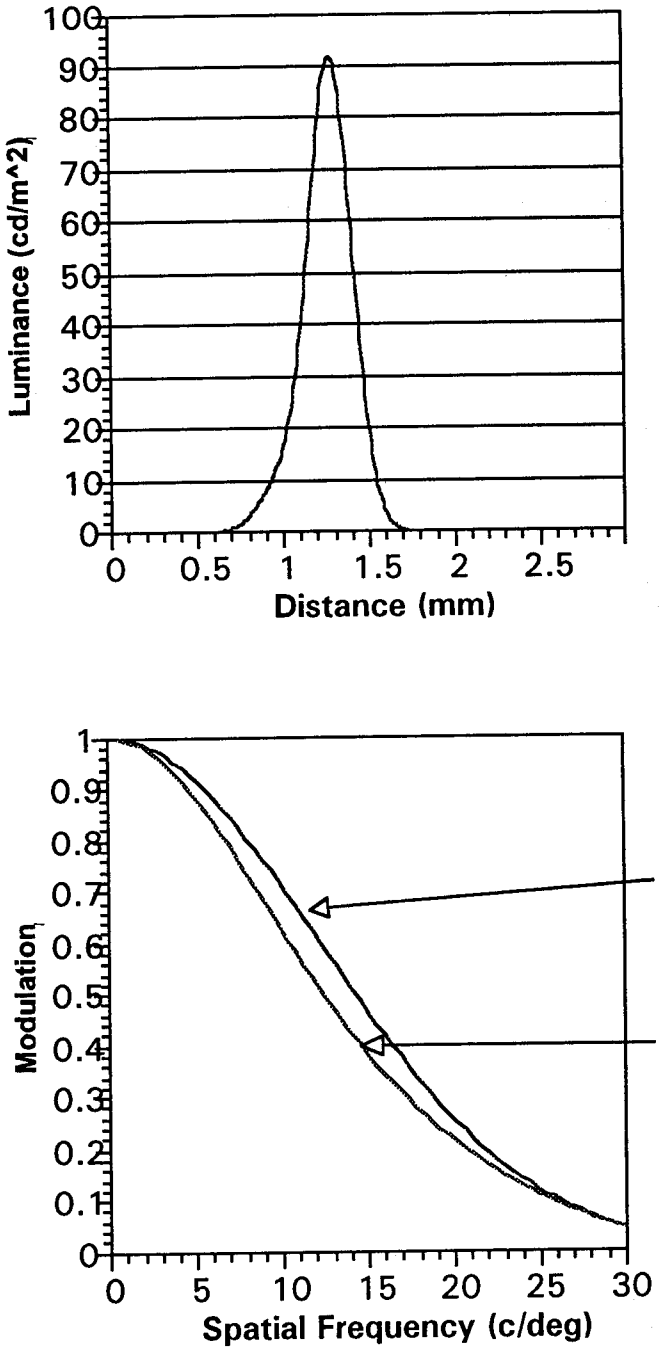

Figure B-21. LSF and Resulting MTF with 0.0 mm of Red Misconvergence and 0.29765 of Blue Misconvergence Compared to the Converged MTF of Figure B1.

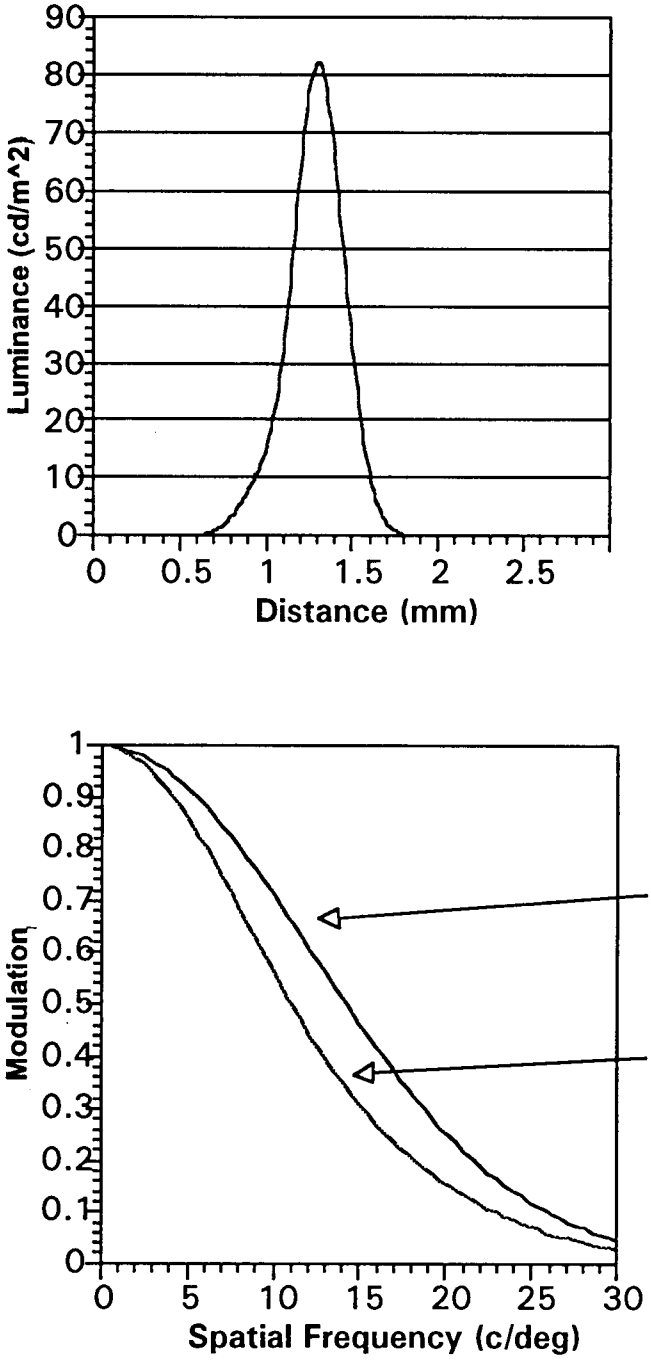

Figure B-22. LSF and Resulting MTF with -0.1488 mm of Red Misconvergence and 0.29765 of Blue Misconvergence Compared to the Converged MTF of Figure B1.

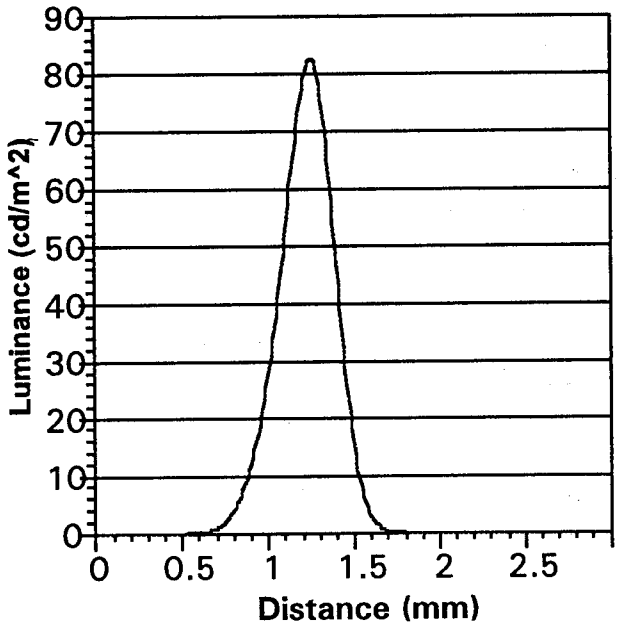

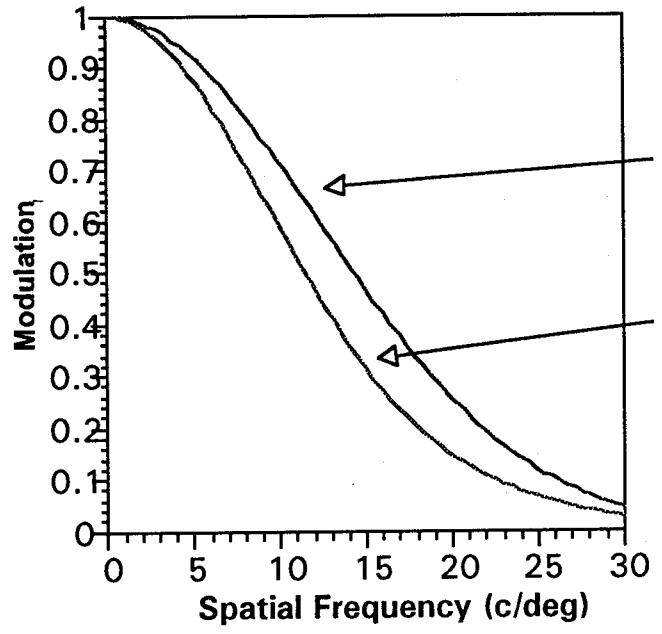

Figure B-23. LSF and Resulting MTF with 0.1488 mm of Red Misconvergence and 0.29765 of Blue Misconvergence Compared to the Converged MTF of Figure B1.

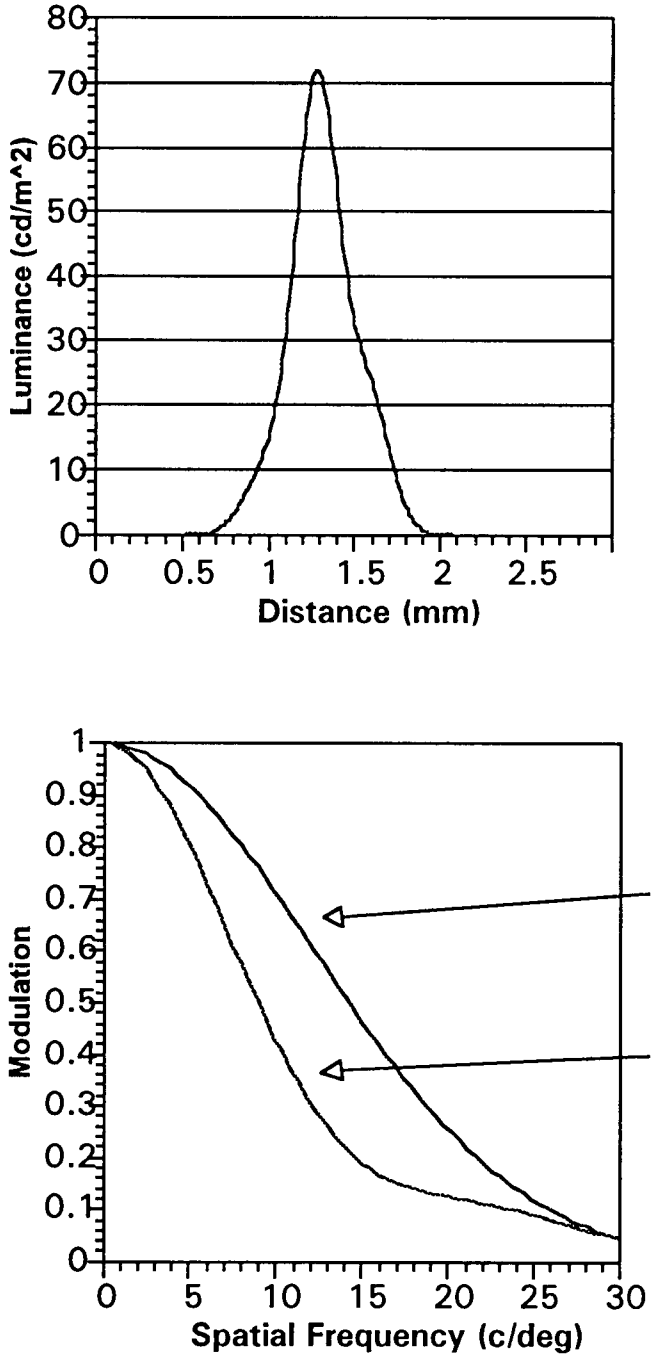

Figure B-24. LSF and Resulting MTF with -0.29765 mm of Red Misconvergence and 0.29765 of Blue Misconvergence Compared to the Converged MTF of Figure B1.

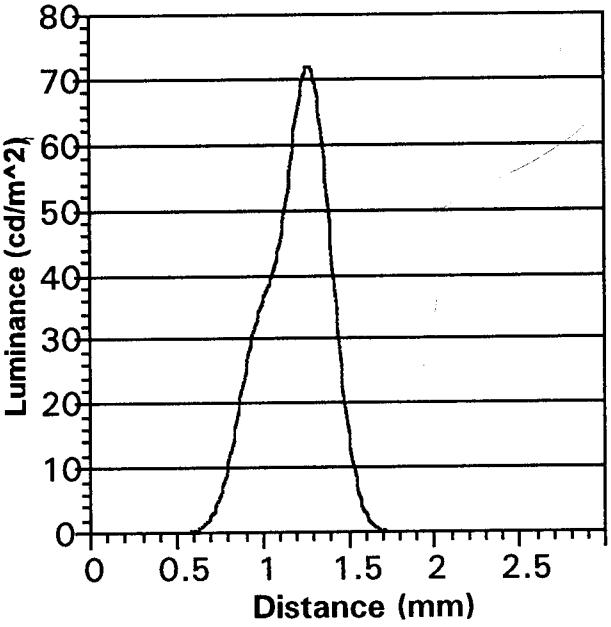

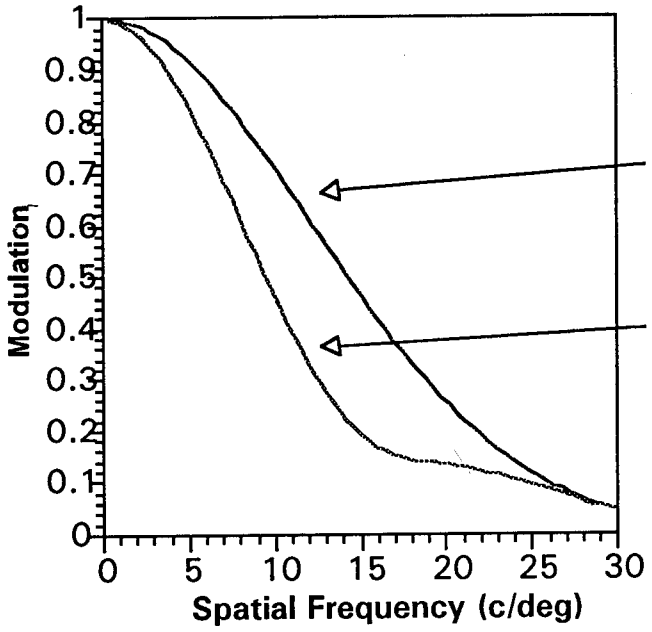

Figure B-25. LSF and Resulting MTF with 0.29765 mm of Red Misconvergence and 0.29765 of Blue Misconvergence Compared to the Converged MTF of Figure B1.